

1 Long-term real-time measurements of aerosol particle composition in
2 Beijing, China: seasonal variations, meteorological effects, and source
3 analysis

4

5 Y. L. Sun^{1*}, Z. F. Wang¹, W. Du^{1,2}, Q. Zhang³, Q. Q. Wang¹, P. Q. Fu¹, X. L. Pan⁴, J. Li¹,
6 J. Jayne⁵, D. R. Worsnop⁵

7

8 *¹State Key Laboratory of Atmospheric Boundary Layer Physics and Atmospheric
9 Chemistry, Institute of Atmospheric Physics, Chinese Academy of Sciences, Beijing
10 100029, China*

11 *²Department of Resources and Environment, Air Environmental Modeling and Pollution
12 Controlling Key Laboratory of Sichuan Higher Education Institutes, Chengdu University
13 of Information Technology, Chengdu 610225, China*

14 *³Department of Environmental Toxicology, University of California, 1 Shields Ave.,
15 Davis, CA 95616*

16 *⁴Research Institute for Applied Mechanics, Kyushu University, Fukuoka, Japan*

17 *⁵Aerodyne Research, Inc., Billerica, MA 01821, USA*

18

19 *Correspondence to Y. L. Sun (sunyele@mail.iap.ac.cn)

20 **Abstract**

21 High concentrations of fine particles ($PM_{2.5}$) are frequently observed during all seasons in
22 Beijing, China, leading to severe air pollution and human health problems in this
23 megacity. In this study, we conducted real-time measurements of non-refractory
24 submicron aerosol (NR- PM_1) species (sulfate, nitrate, ammonium, chloride, and organics) in
25 Beijing using an Aerodyne Aerosol Chemical Speciation Monitor for 1 year, from July
26 2011 to June 2012. This is the first long-term, highly time-resolved (~ 15 min)
27 measurement of fine particle composition in China. The seasonal average ($\pm 1\sigma$) mass
28 concentration of NR- PM_1 ranged from $52 (\pm 49) \mu g m^{-3}$ in the spring season to $62 (\pm 49) \mu g m^{-3}$ in
29 the summer season, with organics being the major fraction (40–51%), followed
30 by nitrate (17–25%) and sulfate (12–17%). Organics and chloride showed pronounced
31 seasonal variations, with much higher concentrations in winter than in the other seasons,
32 due to enhanced coal combustion emissions. Although the seasonal variations of
33 secondary inorganic aerosol (SIA = sulfate + nitrate + ammonium) concentrations were
34 not significant, higher contributions of SIA were observed in summer (57–61%) than in
35 winter (43–46%), indicating that secondary aerosol production is a more important
36 process than primary emissions in summer. Organics presented pronounced diurnal
37 cycles that were similar among all seasons, whereas the diurnal variations of nitrate were
38 mainly due to the competition between photochemical production and gas–particle
39 partitioning. Our data also indicate that high concentrations of NR- PM_1 ($> 60 \mu g m^{-3}$) are
40 usually associated with high ambient relative humidity (RH) ($> 50\%$) and that severe
41 particulate pollution is characterized by different aerosol composition in different
42 seasons. All NR- PM_1 species showed evident concentration gradients as a function of
43 wind direction, generally with higher values associated with wind from the south,
44 southeast or east. This was consistent with their higher potential as source areas, as
45 determined by potential source contribution function analysis. A common high potential
46 source area, located to the southwest of Beijing along the Taihang Mountains, was
47 observed during all seasons except winter, when smaller source areas were found. These
48 results demonstrate a high potential impact of regional transport from surrounding
49 regions on the formation of severe haze pollution in Beijing.

50 **1 Introduction**

51 Severe haze pollution episodes, characterized by high concentrations of fine particles
52 ($PM_{2.5}$), occur frequently during all seasons in China (Sun et al., 2013b; Guo et al., 2014;
53 Zheng et al., 2015), not only reducing visibility significantly, but also exerting harmful
54 effects on public health (Cao et al., 2012). The mass concentrations of $PM_{2.5}$ often far
55 exceed the China National Ambient Air Quality Standard (NAAQS; $75 \mu g m^{-3}$ as a 24-
56 hour average), particularly in the economically developed regions of Beijing–Tianjin–
57 Hebei and Yangtze River Delta (YRD). According to Beijing Environmental Statements,
58 the annual average mass concentration of $PM_{2.5}$ was 89.5 and $85.9 \mu g m^{-3}$ in 2013 and
59 2014, respectively, 2.5 times the NAAQS ($35 \mu g m^{-3}$ as an annual average), indicating
60 that Beijing is still facing severe fine particle pollution. While extensive studies have
61 been conducted in recent years to characterize severe haze pollution (e.g., Guo et al.,
62 2014; Huang et al., 2014; Sun et al., 2014; Zheng et al., 2015), most were carried out in a
63 particular season. In reality, the very different compositions, sources, and evolution
64 processes of severe haze pollution among the different seasons mean that a longer-term
65 approach is needed to meet the challenge of mitigating fine particle pollution in Beijing.

66 A number of long-term measurements and source analyses have been conducted in
67 Beijing during the last decade. Zhao et al. (2009) reported pronounced seasonal variations
68 of $PM_{2.5}$, with higher concentrations in winter than summer. Similarly, Yang et al. (2011)
69 conducted a long-term study of carbonaceous aerosol from 2005 to 2008 in urban
70 Beijing. Both organic carbon (OC) and elemental carbon (EC) showed pronounced
71 seasonal variations, with the highest concentrations occurring in winter and the lowest
72 values in summer. A more detailed investigation of the chemical composition and sources
73 of $PM_{2.5}$ in urban Beijing can be found in Zhang et al. (2013a). Sources of fine particles
74 also vary greatly among the different seasons; for instance, coal combustion during
75 periods requiring more domestic heating, biomass burning in harvest seasons, and dust
76 storms in spring (Zheng et al., 2005; Zhang et al., 2013a). Despite this, most previous
77 long-term studies either focused on limited aerosol species, relied upon weekly filter
78 samples, or used one month's worth of data to represent an entire season (Zhang et al.,
79 2013a; Zhang et al., 2013b). Therefore, our understanding of the full spectrum of
80 seasonal variations of aerosol species and sources remains quite poor.

81 The Aerodyne Aerosol Mass Spectrometer (AMS) is unique in its ability to provide
82 real-time, online measurements of size-resolved submicron aerosol composition (Jayne et
83 al., 2000; Canagaratna et al., 2007). While the AMS has been widely used in China in
84 recent years (Xu et al., 2014a and references therein), real-time, long-term measurements
85 of aerosol particle composition are still rare. Zhang et al. (2013b) conducted a four-month
86 measurement campaign of submicron aerosol composition and size distributions using a
87 quadrupole AMS in urban Beijing. Their results showed higher concentration of organics
88 during wintertime and secondary inorganic species in summer. Furthermore, positive
89 matrix factorization (PMF) analysis of organic aerosol (OA) showed higher primary OA
90 (POA) in winter and secondary OA (SOA) in summer. However, measurements over
91 only one month or even less were conducted for each season, due to the high cost and
92 maintenance of the AMS. The recently developed Aerosol Chemical Speciation Monitor
93 (ACSM) is specially designed for long-term routine measurements of submicron aerosol
94 composition (Ng et al., 2011). The ACSM has been proven reliable by several recent
95 long-term field measurements, e.g., in Paris (Petit et al., 2015), north-central Oklahoma
96 (Parworth et al., 2015), and Santiago de Chile (Carbone et al., 2013). Although the
97 ACSM has been deployed at various sites in China (Sun et al., 2012; Sun et al., 2013b;
98 Zhang et al., 2015), long-term measurements have yet to be reported.

99 In this study, the first of its kind, we conducted long-term, real-time measurements of
100 non-refractory submicron aerosol (NR-PM₁) composition with an ACSM in Beijing,
101 China, from July 2011 to June 2012. The seasonal variations of mass concentration and
102 composition of submicron aerosol were characterized, and the diurnal cycles of aerosol
103 species during the four seasons elucidated. The effects of meteorological parameters,
104 particularly relative humidity and temperature, on aerosol composition and formation
105 mechanisms were investigated. Finally, the potential source areas leading to high
106 concentrations of aerosol species during the four seasons were investigated via potential
107 source contribution function (PSCF) analysis.

108 2 Experimental methods

109 2.1 Sampling site

110 The ACSM was deployed on the roof of a two-story building (~8 m) at the Institute of

111 Atmospheric Physics (IAP), Chinese Academy of Sciences (39°58'28''N, 116°22'16''E,
112 Fig. 1a) from July 2011 to June 2012. The sampling site is located between the north
113 third and fourth ring road in Beijing, which is a typical urban site with influences from
114 local traffic and cooking sources (Sun et al., 2012). The wind rose plots (Fig. 1b) show
115 that southwesterly winds dominate all seasons except winter, when northwesterly and
116 northerly winds prevail. The spring and fall seasons are also characterized by high
117 frequencies of northwesterly and northerly winds. Also note that the prevailing winds
118 with high wind speeds are more frequent during winter and spring than summer.

119 The meteorological parameters, including wind speed (WS), wind direction, relative
120 humidity (RH), and temperature (T) were obtained from a 325 m meteorological tower at
121 the same location. The parameters of pressure (P), solar radiation (SR), and precipitation
122 were obtained from a ground meteorological station located nearby. The monthly
123 variations of these meteorological parameters are presented in Fig. 2. Pronounced
124 seasonal variations were observed for all meteorological parameters except WS. RH
125 averaged at $>\sim 60\%$ in summer and presented its minimum value ($< 30\%$) in February.
126 Temperature and solar radiation showed similar seasonal cycles, with high values in
127 summer and low values in winter. The monthly variations of WS were relatively flat, yet
128 slightly higher values in spring were observed. In addition, a considerable amount of
129 precipitation was observed from June to August, yet it was negligible during wintertime.

130 **2.2 Aerosol and gas measurements**

131 The submicron aerosol particle composition including organics, sulfate, nitrate,
132 ammonium, and chloride was measured *in-situ* by the ACSM at a time resolution of ~ 15
133 min. The ACSM, built upon previous AMSs (Jayne et al., 2000; Drewnick et al., 2005;
134 DeCarlo et al., 2006), is specially designed for long-term routine measurements of fine
135 particle composition (Ng et al., 2011). The ACSM has been successfully deployed at
136 various sites for chemical characterization of submicron aerosol (Ng et al., 2011;
137 Budisulistiorini et al., 2013; Carbone et al., 2013; Sun et al., 2013b; Parworth et al.,
138 2015). In this study, ambient aerosol particles were delivered to the sampling room
139 through a stainless steel tubing (outer diameter: 1.27 cm) with a flow rate of $\sim 3 \text{ L min}^{-1}$,
140 out of which $\sim 84 \text{ cc min}^{-1}$ was sampled into the ACSM. A $\text{PM}_{2.5}$ URG cyclone (URG-

141 2000-30ED) was installed in front of the sampling line to remove coarse particles (> 2.5 μm). To reduce the uncertainties of collection efficiency (CE), a silica gel diffusion dryer
142 was set up in the front of the ACSM to ensure that the aerosol particles sampled were dry
143 ($< 40\%$). The ACSM was calibrated routinely with pure ammonium nitrate particles for
144 the response factor following the procedures detailed in Ng et al. (2011). A more detailed
145 description of the ACSM calibration is given in Sun et al. (2012). It should be noted that
146 we did not calibrate the ACSM with $(\text{NH}_4)_2\text{SO}_4$ to determine the relative ionization
147 efficiency (RIE) of sulfate since such an approach was only proposed recently. Using the
148 method suggested by Budisulistiorini et al. (2014), the RIE of sulfate was estimated to be
149 1.1 – 1.6 during four seasons, leading to a highest uncertainty of 35% in sulfate
150 quantification. Considering that aerosol particle acidity may vary largely between
151 different seasons, the method of Budisulistiorini et al. (2014) may introduce additional
152 uncertainties in sulfate quantification. Therefore, we kept the default RIE of sulfate for
153 the data analysis in this study.

155 **2.3 ACSM data analysis**

156 The ACSM data were analyzed for the mass concentrations of NR-PM₁ species
157 including organics, sulfate, nitrate, ammonium, and chloride using ACSM standard data
158 analysis software. The RH in the sampling line, aerosol particle acidity and the fraction of
159 ammonium nitrate (f_{AN}) in NR-PM₁ are three major factors affecting the uncertainties of
160 CE (Huffman et al., 2005; Matthew et al., 2008; Middlebrook et al., 2012). Because
161 aerosol particles were dry and overall neutralized for most of the time, except some
162 periods when the ratio of measured NH_4^+ to predicted NH_4^+ ($= 2 \times \text{SO}_4^{2-} / 96 \times 18 +$
163 $\text{NO}_3^- / 62 \times 18 + \text{Cl}^- / 35.5 \times 18$) (Zhang et al., 2007) was less than 0.8, the composition
164 dependent CE recommended by Middlebrook et al. (2012), which is $\text{CE} = \max(0.45,$
165 $0.0833 + 0.9167 \times f_{\text{AN}})$, was used in this study. The validity of the ACSM data using
166 variable CE in summer and winter was reported previously in Sun et al. (2012) and Sun
167 et al. (2013b) by comparing the NR-PM₁ with PM_{2.5} mass concentration measured by a
168 TEOM system. The correlation between NR-PM₁ and PM_{2.5} for the entire year is shown
169 in Fig. S1. The measured NR-PM₁ overall tracked well with that of PM_{2.5}, and yet
170 showed different slopes in different seasons. The average ratio of NR-PM₁/PM_{2.5} for the
171 entire year was 0.77 ($r^2 = 0.66$). It should be noted that the PM_{2.5} was measured by a

172 heated TEOM (50°C), which might have caused significant losses of semi-volatile
173 species, e.g., ammonium nitrate and semi-volatile organics. For example, Docherty et al.
174 (2011) found an average loss of ~44% PM_{2.5} mass through use of the heated TEOM
175 compared to that measured with a filter dynamics measurement system. Assuming that
176 the average loss of PM_{2.5} mass by the heated TEOM is 30–50%, the NR-PM₁/PM_{2.5} ratio
177 for the entire study would be ~0.5–0.6, which is close to that reported in Zhang et al.
178 (2013b). Figure S1 also shows large variations of NR-PM₁/PM_{2.5} ratios in the different
179 seasons. The reasons for the variations include: 1) the ACSM cannot detect refractory
180 black carbon, mineral dust, and metals. For example, low ratios of NR-PM₁/PM_{2.5} (< 0.3)
181 were observed during dust storm periods, when mineral dust is the dominant component
182 of fine particles; 2) the contribution of semi-volatile species to PM_{2.5} varied greatly
183 among the different seasons; and 3) the contribution of particles in the range of 1–2.5 µm
184 to the total PM_{2.5} might also be different among different pollution episodes.

185 **2.4 PSCF analysis**

186 The 72 hr back trajectories arriving at the IAP study site at a height of 300 m were
187 calculated every 3 hr for the entire study period using the National Oceanic and
188 Atmospheric Administration Hybrid Single-Particle Lagrangian Integrated Trajectory
189 model, version 4.8 (Draxler and Rolph, 2003). Each trajectory contained a series of
190 latitude-longitude coordinates every 1 h backward in time for 72 hr. If a trajectory end
191 point falls into a grid cell (i, j), the trajectory is assumed to collect material emitted in the
192 cell (Polissar et al., 1999). The number of end points falling into a single grid cell is n_{ij} .
193 Some of these trajectory end points are associated with the data with the concentration of
194 aerosol species higher than a threshold value. The number of these points is m_{ij} . The
195 potential source contribution function (PSCF) is then calculated as the ratio of the
196 number of points with concentration higher than a threshold value (m_{ij}) to the total
197 number of points (n_{ij}) in the ij -th grid cell. Higher PSCF values indicate higher potential
198 source contributions to the receptor site. In this study, the domain for the PSCF was set in
199 the range of (34–44°N, 110–124°E). The 75th percentile for each aerosol species during
200 the four seasons (Table S1) was used as the threshold value to calculate m_{ij} . To reduce the
201 uncertainties of m_{ij}/n_{ij} for those grid cells with a limited number of points, a weighting

202 function (w_{ij}) recommended by Polissar et al. (1999) was applied to the PSCF in each
203 season.

$$w_{ij} = \begin{cases} 1.00 & 80 < n_{ij} \\ 0.70 & 20 < n_{ij} \leq 80 \\ 0.42 & 10 < n_{ij} \leq 20 \\ 0.05 & n_{ij} \leq 10 \end{cases}$$

204 **3 Results and discussion**

205 **3.1 Mass concentration and chemical composition**

206 The average mass concentration of NR-PM₁ was 62 $\mu\text{g m}^{-3}$ in summer (Fig. 3),
207 which is higher than the 50 $\mu\text{g m}^{-3}$ for July–August 2011 reported in Sun et al. (2012)
208 due to the biomass burning impacts in June 2012 (Fig. S2). The summer NR-PM₁ level is
209 close to that measured by a High Resolution Aerosol Mass Spectrometer during the
210 Beijing 2008 Olympic Games (Huang et al., 2010), but ~20% lower than that determined
211 in summer 2006 (Sun et al., 2010). The average NR-PM₁ mass concentrations were
212 relatively similar during the other three seasons, varying from 52 to 59 $\mu\text{g m}^{-3}$ and with
213 slightly higher concentration during wintertime (Fig. 3). The NR-PM₁ measured in urban
214 Beijing is overall higher than those previously reported in the Yangtze River Delta
215 (YRD) region (27–43 $\mu\text{g m}^{-3}$) (Huang et al., 2012; Huang et al., 2013; Zhang et al., 2015)
216 and Pearl River Delta (PRD) region (31–48 $\mu\text{g m}^{-3}$) (He et al., 2011; Huang et al., 2011;
217 Gong et al., 2012), indicating more severe submicron aerosol pollution in Beijing
218 compared to other places in China. Indeed, the annual average NR-PM₁ concentration (57
219 $\mu\text{g m}^{-3}$) was much higher than the China NAAQS of PM_{2.5} (35 $\mu\text{g m}^{-3}$ as an annual
220 average). Assuming a similar PM_{2.5} level as that (89.5 $\mu\text{g m}^{-3}$) in Beijing in 2013, NR-
221 PM₁ on average accounted for 64% of PM_{2.5}, which is overall consistent with the results
222 reported in previous studies (Sun et al., 2012; Sun et al., 2013b; Zhang et al., 2013b).

223 As indicated in Fig. 4, the summer season showed the highest frequency with NR-
224 PM₁ loading in the range of 30–60 $\mu\text{g m}^{-3}$ (36% of the time), while the winter season
225 presented the highest frequency of low mass loadings (< 20 $\mu\text{g m}^{-3}$, 34% of the time) due
226 to the prevailing northwesterly winds (Fig. 1b). However, high NR-PM₁ loading (> 90 μg
227 m^{-3}) occurred 31% of the time during the winter season, substantially more than during

any of the other seasons (25%, 25% and 21% during summer, fall and spring, respectively), indicating that heavy pollution occurred more frequently during winter than the other seasons. The fall and spring seasons showed similar variations of frequencies, which overall decreased monotonically as a function of NR-PM₁ loadings. Note that heavily polluted events, with NR-PM₁ mass concentrations larger than 150 $\mu\text{g m}^{-3}$, occurred during all seasons, on average accounting for 3–7% of the total time. Such heavily polluted events were mainly caused by agricultural burning in summer and fall, and coal combustion in winter, particularly under stagnant meteorological conditions (Sun et al., 2013b; Cheng et al., 2014).

The NR-PM₁ species varied dramatically and differently during the four seasons (Fig. 3). Overall, organics dominated NR-PM₁ during all seasons, accounting for 40–51% on average. The dominance of organics in NR-PM₁ has been widely observed at various sites in China, e.g., 31–52% in the YRD region (Huang et al., 2012; Huang et al., 2013; Zhang et al., 2015), 36–46% in the PRD region (He et al., 2011; Huang et al., 2011; Gong et al., 2012), and 47% in northwest China (Xu et al., 2014a). Organics showed the largest contribution to NR-PM₁ in winter due to a large amount of carbonaceous aerosol emitted from coal combustion (Chen et al., 2005; Zhang et al., 2008). This is also consistent with the highest contribution of chloride, with coal combustion being a major source in winter (Zhang et al., 2012). High concentrations of organics were also observed during late June and early October, due to the impacts of agricultural burning in these two months. Secondary inorganic aerosol (SIA = sulfate + nitrate + ammonium) contributed the largest fraction of NR-PM₁ during the summer season (59%) and the lowest fraction during the winter season (44%). Such seasonal differences in PM composition reflect the different roles played by primary emissions and secondary formation. While photochemical production of secondary aerosol associated with higher O₃ and stronger solar radiation (Fig. 2) plays a dominant role in affecting aerosol composition in summer, primary emissions play enhanced roles in winter when photochemical processing is weaker (Sun et al., 2013b). It is interesting to note that nitrate, on average, showed a higher contribution than sulfate during the four seasons. Compared to previous AMS measurements in Beijing (Huang et al., 2010; Sun et al., 2010), the nitrate contribution to NR-PM₁ appears to show an increasing trend. The ratio of NO₃[−]/SO₄^{2−} varied from 1.3–

259 1.8 in this study, which is overall higher than those (0.8–1.5) observed during the four
260 seasons in 2008 (Zhang et al., 2013b). This result likely indicates a response of secondary
261 inorganic aerosol composition to the variations of precursors of NO_x and SO_2 in recent
262 years. For instance, a continuous effort to reduce SO_2 emissions is accompanied with a
263 gradual increase in NO_x emissions (Wang et al., 2014b), which results in an increasingly
264 more important role played by nitrate in PM pollution in Beijing. Indeed, a recent model
265 analysis of the response of SIA to their precursors from 2000–2015 showed that the
266 increase of nitrate would exceed the reduction of sulfate in northern China, assuming no
267 change to NH_3 emissions (Wang et al., 2013). A higher concentration of nitrate than
268 sulfate has also been frequently observed at urban and rural sites in China in recent years,
269 e.g., Nanjing, in the YRD region (Zhang et al., 2015), and Changdao Island (Hu et al.,
270 2013).

271 **3.2 Seasonal variation**

272 The monthly average NR- PM_1 mass concentration stayed relatively constant
273 throughout the year, with the average value ranging from 46 to $60 \mu\text{g m}^{-3}$, except in June
274 2012 (Fig. 5). The month of June presented the highest NR- PM_1 ($89 \mu\text{g m}^{-3}$) due to the
275 impact of agricultural burning. Consistently, a higher concentration of NR- PM_1 was
276 observed in the summer of 2008 (5 June – 3 July) than the other seasons in Beijing
277 (Zhang et al., 2013b). Zhao et al. (2009) also observed the highest concentration of $\text{PM}_{2.5}$
278 in June 2007, due to the influences of agricultural burning. These results indicate that
279 agricultural burning is a large source of PM pollution in Beijing in summer. The lowest
280 concentration of NR- PM_1 in summer occurred in July, mainly due to the abundant
281 precipitation and high temperatures, which facilitated wet scavenging and convection of
282 PM, respectively (Fig. 2). Similarly lower concentrations of $\text{PM}_{2.5}$ in summer than in the
283 other seasons were also observed previously at an urban site in Beijing (Zhao et al.,
284 2009).

285 Among the NR aerosol species, organics and chloride presented pronounced seasonal
286 variations, showing higher concentrations in winter than in the other seasons (Fig. 5). The
287 concentration of organics increased from $17 \mu\text{g m}^{-3}$ in July to $\sim 30 \mu\text{g m}^{-3}$ in October, and
288 then remained relatively stable across the whole of wintertime. The concentration of

289 organics reached a minimum in April ($17 \mu\text{g m}^{-3}$), and then rapidly increased to $37 \mu\text{g}$
290 m^{-3} in June. Correspondingly, the contribution of organics to NR-PM₁ increased from
291 ~40% in summer to above 50% during wintertime (Fig. 6). A higher concentration of
292 carbonaceous aerosol in winter, compared to the other three seasons, was also observed
293 in Beijing (Zhang et al., 2013a; Zhao et al., 2013). The seasonal variation of organics is
294 primarily driven by emissions from various sources and secondary production. While the
295 POA, particularly from coal combustion emissions, is significantly elevated during
296 wintertime, the photochemically processed SOA dominates OA in summer (Sun et al.,
297 2012; Sun et al., 2013b). In the present study, chloride showed a similar seasonal
298 variation to that of organics. The chloride concentration during wintertime ($2.8\text{--}3.3 \mu\text{g}$
299 m^{-3}) was approximately six times that ($0.5 \mu\text{g m}^{-3}$) in summer. The contribution of
300 chloride to NR-PM₁ showed a similar seasonal trend, with the lowest contribution in
301 summer (~1%) and the highest in winter (~5–6%) (Fig. 6). High concentrations of
302 chloride in winter are associated with enhanced coal combustion emissions (Sun et al.,
303 2013b), but also with low ambient temperature, which facilitates the formation of
304 particle-phase ammonium chloride. Also note that chloride showed a twice as high
305 concentration and contribution in June than the other two months in summer because
306 agricultural burning is also a large source of chloride (Viana et al., 2008; Cheng et al.,
307 2014).

308 The seasonal variation of sulfate is different from organics and chloride. The sulfate
309 concentration gradually decreased from $10.1 \mu\text{g m}^{-3}$ in August to $4.9 \mu\text{g m}^{-3}$ in
310 November, which was associated with a synchronous decrease in solar radiation and O₃
311 (Fig. 2). The contribution of sulfate to NR-PM₁ showed a corresponding decrease from
312 19% to 10%. The sulfate concentration then increased to $8.3\text{--}8.8 \mu\text{g m}^{-3}$ in December
313 and January, likely due to a significant increase of precursor SO₂ associated with an
314 increased demand for domestic heating during the winter season, which can be oxidized
315 to form sulfate via either gas-phase oxidation or aqueous-phase processing (Xu et al.,
316 2014b). Sulfate showed the highest concentration in June ($13.5 \mu\text{g m}^{-3}$) due to secondary
317 production, but possibly the impact of biomass burning as well. Indeed, a recent study in
318 the YRD region also found a large enhancement of sulfate in biomass burning plumes in
319 summer (Zhang et al., 2015). Nitrate showed minor seasonal variation, with the monthly

320 average concentration ranging from 8 to 15 $\mu\text{g m}^{-3}$, except in June (23 $\mu\text{g m}^{-3}$). It is
321 interesting that a higher concentration of nitrate was observed in summer and spring than
322 in winter. On average, nitrate accounted for ~25% of NR-PM₁ during summertime, but
323 decreased to ~15% during wintertime (Fig. 6). Although high temperatures in summer
324 favor the dissociation of ammonium nitrate particles to gas-phase ammonia and nitric
325 acid, the correspondingly high RH and excess gaseous ammonia facilitate the
326 transformation of nitric acid to aqueous NH₄NO₃ particles (Meng et al., 2011; Sun et al.,
327 2012). The lowest concentration of nitrate during wintertime might be primarily caused
328 by the weak photochemical production associated with low solar radiation and oxidants
329 (e.g., O₃). In addition, the higher particle acidity in winter (Liu, 2012) and lower mixing
330 ratio of gaseous ammonia may also suppress the formation of ammonium nitrate particles
331 (Zhang et al., 2007). The seasonal variation of ammonium is similar to that of sulfate and
332 nitrate because ammonium primarily exists in the form of NH₄NO₃ and (NH₄)₂SO₄.

333 3.3 Diurnal variations

334 As demonstrated in Fig. 7, the diurnal cycles of organics during the four seasons were
335 overall similar, characterized by two pronounced peaks occurring at noon and during the
336 evening time. PMF analysis of OA suggested that the noon peak was primarily caused by
337 cooking emissions, while the evening peak was driven by different primary emissions
338 (e.g., cooking, traffic, and coal combustion emissions) among the different seasons (Sun
339 et al., 2012; Sun et al., 2013b). It should be noted that the noon peak in summer was more
340 significant than in fall and winter. Indeed, the cooking emissions, determined by
341 subtracting the background (10:00–11:00) from the noon peak (12:00–13:00), were ~1.5–
342 2 $\mu\text{g m}^{-3}$ from September to the following March, which were lower than the ~3.5 $\mu\text{g m}^{-3}$
343 calculated for June and July. This seasonal trend agreed with that of temperature,
344 indicating that cooking emissions are temperature dependent, probably because of
345 increased cooking activity in hot summers than cold winters.

346 Relatively flat diurnal cycles were observed for sulfate during most months,
347 indicating the regional characteristics of sulfate. In fact, multi-day build-up of sulfate was
348 frequently observed during all seasons (Fig. 3), supporting the notion of regional
349 influences on sulfate in Beijing. It should be noted that the daytime photochemical

350 production of sulfate from gas-phase oxidation of SO_2 might be masked by an elevated
351 planetary boundary layer (PBL). Considering the dilution effect of the PBL, Sun et al.
352 (2012) found that sulfate increased gradually from morning to late afternoon,
353 demonstrating the daytime photochemical production of sulfate. In this study, sulfate in
354 May, June and October showed an evident daytime increase until late afternoon,
355 indicating an important role played by gas-phase photochemical processing in driving the
356 sulfate diurnal cycle.

357 Nitrate showed substantially different diurnal cycles among different months. A clear
358 daytime increase starting from about 8:00 to 19:00 was found in the five months of
359 January, February, March, November and December, indicating that such a diurnal
360 pattern is more significant during wintertime compared to the fall and spring seasons.
361 Figure 2 shows that the temperature during these five months was generally low (<
362 10°C), under which the partitioning of NH_4NO_3 into gaseous NH_3 and HNO_3 would not
363 be significant. As a result, photochemical production would be the primary factor driving
364 the diurnal variations. The photochemical production rate calculated from the daytime
365 increase was $0.6\text{--}0.8 \mu\text{g m}^{-3} \text{ hr}^{-1}$ during winter and $\sim 0.2\text{--}0.3 \mu\text{g m}^{-3} \text{ hr}^{-1}$ in November
366 and March. Nitrate presented pronounced diurnal cycles in summer (June, July and
367 August), with the concentrations gradually decreasing during daytime and reaching a
368 minimum at $\sim 16:00$. Similar diurnal cycles have been observed on many occasions in
369 summer in Beijing (Huang et al., 2010; Sun et al., 2012; Zhang et al., 2015). The
370 evaporative loss of NH_4NO_3 associated with high temperatures, which overcomes the
371 amount of photochemical production, plays the major role in driving such diurnal cycles.
372 The rising PBL plays an additional role in the low concentrations of nitrate during
373 daytime (Sun et al., 2012). The diurnal cycle of nitrate in May and September was also
374 significant, characterized by a pronounced morning peak occurring at $\sim 10:00$, when
375 photochemical production dominated over the gas–particle partitioning of NH_4NO_3 .
376 Nitrate showed a relatively flat diurnal cycle in April, indicating a combined effect of
377 various nitrate formation mechanisms.

378 Chloride in this study was primarily detected as ammonium chloride because ACSM
379 is insensitive to refractory NaCl and/or KCl at its vaporizer temperature of 600°C . As
380 shown in Fig. 7, two different diurnal cycles were observed throughout different months.

381 For the months of July, August, September, April and May, chloride presented a morning
382 peak when both temperatures and the PBL were at their lowest, and then rapidly
383 decreased to a low ambient level at ~18:00. Such a diurnal cycle was likely primarily
384 driven by temperature dependent gas–particle partitioning (Hu et al., 2008). The diurnal
385 cycles of chloride during the remaining months were also significant, all of which were
386 characterized by high concentrations at night. Coincidentally, these months fell during
387 the season of high domestic-heating demand, which usually starts on 15 November and
388 ends on 15 March. Coal combustion has been found to be a large source of chloride
389 (Zhang et al., 2012; Sun et al., 2013b). Therefore, the diurnal cycle of chloride is likely
390 dominantly driven by coal combustion emissions that are intensified at night for domestic
391 heating.

392 **3.4 Weekend effects**

393 Because the switch between clean periods and pollution episodes arising from
394 different source areas happens frequently in Beijing (Sun et al., 2013b; Guo et al., 2014),
395 the diurnal cycles of aerosol species can vary greatly due to the influences of different
396 occurrences of clean periods between weekdays and weekends (Sun et al., 2013b).
397 Therefore, periods with low aerosol loadings ($\text{NR-PM}_1 < 20 \mu\text{g m}^{-3}$) were excluded from
398 the results (Fig. 8) for a better investigation of the weekend effects (for the average
399 diurnal cycles with clean periods included, see Fig. S3). As shown in Fig. 8, there were
400 no clear weekend effects in the summer, except for slightly lower concentrations of
401 organics, sulfate and nitrate in the late afternoon on weekends. This suggests that there
402 are no significant differences in anthropogenic activity between weekdays and weekends
403 in summer. Although some enhanced traffic emissions between 00:00 and 06:00 on
404 weekends might have occurred, as indicated by the higher concentration of NO (Fig. S4),
405 they appeared to have negligible impacts on secondary sulfate and nitrate. While the
406 diurnal variations of organics and chloride were similar between weekdays and weekends
407 during the fall season, sulfate and nitrate showed pronounced weekend effects, with
408 persistently higher concentrations at weekends throughout the day. An explanation for
409 this is the stronger photochemical production of secondary species associated with higher
410 O_3 and solar radiation on weekends (Fig. S4). Consistently, SOA showed similar
411 weekend effects as those of secondary inorganic species, while POA did not (Sun et al.,

412 in preparation). Because of the regional characteristics of secondary aerosols, further
413 analysis is needed to address the impacts of regional transport on the weekend effects of
414 secondary species. Winter showed the most pronounced weekend effects for all aerosol
415 species. All aerosol species showed much lower concentrations on weekends than on
416 weekdays across the entire day, which was consistent with those of NO, SO₂, and CO
417 (Fig. S4). These results clearly indicate much reduced anthropogenic activity on
418 weekends during wintertime because of low ambient temperature (−4°C to −3°C).
419 Further evidence is provided by the diurnal cycles of organics, which presented
420 pronounced noon peaks on weekends during all seasons except winter. This observation
421 was consistent with much reduced cooking activity on weekends during wintertime.
422 Similar to summer, no evident weekend effects were observed in spring. The weekend
423 effects of aerosol species in this study are overall consistent with those observed by Han
424 et al. (2009), in which similar diurnal cycles of primary elemental carbon, CO, and CO₂
425 between weekdays and weekends under weak wind conditions were observed during the
426 three seasons other than winter.

427 **3.5 Meteorological effects**

428 Figure 9 shows the RH and *T* dependent distributions of NR-PM₁ and WS for the
429 entire year. The distribution of NR-PM₁ showed an obvious concentration gradient as a
430 function of RH. NR-PM₁ showed the lowest mass loading, generally less than 20 $\mu\text{g m}^{-3}$
431 at RH < 20%, and had no clear dependence on *T*. This can be explained by the high WS
432 (often larger than 5 m s^{-1} ; Fig. 9b) at low RH levels associated with clean air masses
433 from the north and/or northwest. Previous studies have also found a strong association
434 between low aerosol loading and high WS in Beijing (Han et al., 2009; Sun et al., 2013b).
435 NR-PM₁ showed moderately high concentrations (\sim 20–40 $\mu\text{g m}^{-3}$) at low RH (20–40%),
436 which rapidly increased to a high concentration level ($> 60 \mu\text{g m}^{-3}$) at RH > 50%. These
437 results indicate that severe haze episodes in Beijing mostly occur under high humidity
438 conditions, when WS is low as well. Two different regions with high concentrations of
439 NR-PM₁ are apparent in Fig. 9a: one in the top-right region with high temperature
440 ($>\sim 15^\circ\text{C}$), and another in the bottom-right region with low ambient temperature ($<\sim 6^\circ\text{C}$).
441 Such a difference in distribution illustrates the severity of PM pollution in different

442 seasons. Note that low concentrations of NR-PM₁ sometimes occurred at RH > 90%,
443 likely due to the scavenging of particles by rain or winter snow.

444 The RH- and *T*-dependent distributions of major aerosol species (Fig. 10) allow us to
445 further investigate the RH/*T* impacts on the formation of aerosol species. While all
446 aerosol species showed similar concentration gradients as a function of RH to that of NR-
447 PM₁, the *T*-dependent patterns varied greatly. Organics generally showed the highest
448 concentrations under low *T* (< 6°C) and high humidity conditions – very similar to the
449 behavior of chloride, which is mainly derived from combustion sources, e.g., coal
450 combustion or biomass burning (Zhang et al., 2012; Cheng et al., 2014). The results
451 suggest that high concentrations of organics during wintertime are primarily caused by
452 coal combustion emissions during the domestic-heating season, particularly from
453 residential coal combustion (Zhang et al., 2008). In fact, a previous study by our group
454 found that nearly one-third of OA during wintertime is primary coal combustion OA
455 (CCOA) (Sun et al., 2013b). In contrast, organics showed much lower concentrations
456 under the conditions of higher RH and higher *T*, for which one of the reasons was
457 probably far fewer coal combustion emissions during summertime (Zheng et al., 2005;
458 Zhang et al., 2013a). Consistently, CCOA has not yet been resolved from PMF analyses
459 of AMS OA in summer in Beijing (Huang et al., 2010; Sun et al., 2010). Note that the
460 region with a high concentration of organics corresponded to a high concentration of NR-
461 PM₁. In this region, organics accounted for the largest fraction of NR-PM₁
462 (approximately 40–50%), indicating that severe PM pollution under low temperature and
463 high humidity conditions is dominantly contributed to by organics. The mass fraction of
464 organics, however, showed an opposite distribution to that of mass loading. As shown in
465 Fig. 10, organics presents the highest contribution to NR-PM₁ (~ > 50%) in the left-hand
466 region with low RH, indicating the dominance of organics during periods with low NR-
467 PM₁ mass loadings. Such a distribution is independent of temperature, suggesting a
468 ubiquitously organics-dominant composition during clean days in all seasons.

469 The RH/*T* dependence of secondary inorganic species showed somewhat different
470 behaviors from that of organics. Sulfate presented two high concentration regions, with
471 the highest values occurring during wintertime when *T* was below 0°C and RH was
472 above 70%. Aqueous-phase oxidation, mostly fog processing, has been found to play a

473 dominant role in sulfate formation under such meteorological conditions (Sun et al.,
474 2013a). Surprisingly, the semi-volatile nitrate showed a relatively homogeneous
475 distribution across different temperatures at RH > 40%. Despite high temperature in
476 summer, high humidity facilitates the transformation of gaseous species into aqueous-
477 phase nitrate particles (Sun et al., 2012), particularly in the presence of high abundance of
478 gaseous ammonia (Ianniello et al., 2010). In fact, nitrate showed the highest contribution
479 (>~25%) to NR-PM₁ mass under high *T* and high RH conditions, which were also the
480 conditions under which high concentrations of NR-PM₁ were observed. The fact that
481 nitrate contributed more than sulfate (~15–20%) to NR-PM₁ mass during these conditions
482 suggests an important role played by nitrate in summer haze formation. While the
483 concentration of nitrate at various temperatures was similar, its contribution to NR-PM₁
484 was generally lower at low temperatures due to the greater enhancement of organics
485 during wintertime. Also note that the two semi-volatile species, i.e., nitrate and chloride,
486 show the lowest contributions to NR-PM₁ in the top-left region with the highest *T* and
487 lowest RH. This illustrates the evaporative loss process of ammonium nitrate and
488 ammonium chloride under high temperatures in summertime. However, sulfate shows a
489 relatively higher contribution in this region since ammonium sulfate is less volatile than
490 ammonium nitrate and chloride (Huffman et al., 2009).

491 **3.6 Source analysis**

492 In summer, all NR-PM₁ species showed evident wind sector gradients, with higher
493 concentrations in association with winds from the east (E) and southeast (SE), and lower
494 concentrations with northwest (NW) wind (Fig. 11). The average NR-PM₁ concentration
495 from the SE was 89.5 $\mu\text{g m}^{-3}$, which was more than twice that (39.4 $\mu\text{g m}^{-3}$) from the
496 NW. All aerosol species increased as wind sectors changed along the N–NE–E–SE
497 gradient, and then decreased along the SE–S–SW–W gradient. Such wind sector
498 dependence of aerosol composition is remarkably consistent with the spatial distribution
499 of fine particles in Beijing in 2013 (Beijing Environmental Statement 2013). These
500 results suggest an inhomogeneous distribution of air pollution around the IAP sampling
501 site in summer. Organics dominated NR-PM₁ across different sectors (37–43%), followed
502 by nitrate (21–28%), sulfate (15–20%), and ammonium (15–17%). While chloride
503 contributed a small fraction of NR-PM₁ (0.7–1.8%), the mass concentration showed the

504 largest difference between SE and NW. The fall season showed a similar aerosol
505 composition dependence as that in summer, with higher concentrations from the E, SE,
506 and S. However, the gradients of wind sectors appeared to be smaller. For example, the
507 average NR-PM₁ concentration ranged from 46.3 to 72.7 $\mu\text{g m}^{-3}$ in all eight sectors
508 except NW. Organics showed a similar dominance in NR-PM₁, accounting for 47–55%,
509 and the contribution was ubiquitously higher than in summer for all wind sectors. It
510 should be noted that the NW sector showed the largest difference between mean and
511 median values for all species. The much lower median values suggest a dominance of
512 clean days for most of the time in this sector. In contrast, the summer season showed
513 higher median concentrations from the NW, indicating a higher regional background
514 during this season. The winter season showed consistently high concentrations of PM
515 across the different wind sectors, except for NW, where the mass concentrations were
516 approximately half of those in the other sectors. The average NR-PM₁ ranged from 55.0
517 to 84.4 $\mu\text{g m}^{-3}$, with organics being the major fraction, accounting for 46–54%. The
518 spring season showed a similar wind sector dependence on aerosol composition as the
519 fall season. The average NR-PM₁ ranged from 49.0 to 74.4 $\mu\text{g m}^{-3}$ for all of the wind
520 sectors except the N (38.5 $\mu\text{g m}^{-3}$) and NW (24.7 $\mu\text{g m}^{-3}$), which had much lower mass
521 concentrations. Similar to other seasons, organics dominated NR-PM₁ throughout the
522 different sectors (36–53%), followed by nitrate (19–27%) and sulfate (11–16%).

523 As Fig. 12 shows, the potential source areas for aerosol species varied among the four
524 seasons. In summer, high potential source areas were mainly located to the south,
525 southwest and southeast of Beijing. Organics had a relatively small high potential source
526 region in the south of Beijing (< 100 km) and a small source region located around
527 Baoding – one of the most polluted cities in Hebei Province. A narrow and visible source
528 area to the southeast of Beijing, including Tianjin and the Bohai Sea, was also observed.
529 Nitrate and chloride showed similar source areas to organics. The high potential source
530 area to the southeast of Beijing was mainly caused by open agricultural burning in June
531 in northern China. Sulfate showed a distinct source region characterized by a narrow high
532 PSCF band along Hengshui–Baoding–Langfang–Beijing. Such a pollution band agrees
533 well with the topography of the North China Plain, with the Taihang Mountains to the
534 west and Yan Mountains to the north. The wide area of high PSCF for sulfate also

535 indicates a regional characteristic of sulfate that is formed from gas-phase oxidation or
536 cloud processing of precursor SO_2 , which is particularly high in Hebei Province (Ji et al.,
537 2014). Secondary nitrate showed a similar, yet much smaller, PSCF region compared to
538 sulfate. One reason for this might be the evaporative loss of ammonium nitrate during the
539 long-range transport in summer.

540 All aerosol species showed similar PSCF spatial distributions during the fall season,
541 with high potential source regions located in a narrow area from Hengshui, Baoding to
542 Beijing. These results suggest that regional transport from the southwest plays a
543 dominant role in formation of severe haze pollution in fall. The wintertime results
544 showed largely different PSCF distributions from the other seasons. High PSCF values
545 were mainly located in a small region ($< 50 \text{ km}$) in the south and southeast of Beijing.
546 Although Hebei Province often has worse air pollution than Beijing during wintertime (Ji
547 et al., 2014), the cities far away from Beijing appear not to be a very important source of
548 wintertime air pollution in Beijing. One explanation for this is that stagnant
549 meteorological conditions occur more frequently in winter due to low WS and T
550 inversions. Thus, local emissions and transport from nearby regions would play a more
551 significant role in affecting the pollution level in Beijing. While the spring season showed
552 similarly small high potential source regions to those during wintertime, an obvious high
553 potential source area in Hebei Province was also observed. The transport of air pollution
554 from the SW to the NE along the Taihang Mountains in northern China has been
555 observed many times in previous studies (Wang et al., 2014a; Wang et al., 2014c). Given
556 that many cities located on this pathway are often highly polluted, such as
557 Shijiazhuang, Baoding, and Hengshui, regional transport from these areas would have
558 a potentially high impact on the formation of severe haze pollution in Beijing.

559 **4 Conclusion**

560 This paper presents the results from a year-long, real-time measurement study of
561 submicron aerosol particle composition using an ACSM, conducted at an urban site in
562 Beijing from July 2011 to June 2012. The mass concentration of NR- PM_1 varied
563 dramatically, with the seasonal average concentration ranging from 52 to $62 \mu\text{g m}^{-3}$.
564 Organics comprised a major fraction of NR- PM_1 during all seasons, accounting for 40–

565 51% on average. The average contribution of nitrate to NR-PM₁ (17–25%) exceeded that
566 of sulfate (12–17%) during all seasons, suggesting an enhanced role of nitrate in PM
567 pollution in recent years. Organics and chloride were two species showing pronounced
568 seasonal variations in both mass concentrations and mass fractions. The higher
569 concentrations of organics and chloride in winter than summer were largely due to
570 enhanced coal combustion emissions. We also observed high concentrations of organics
571 and chloride in June and October – two months with strong agricultural burning impacts.
572 The seasonal variations of secondary sulfate and nitrate were not significant because of
573 the large variations of precursor concentrations, photochemical production, and also
574 meteorological effects in different seasons. However, higher contributions of SIA in
575 summer (57–61%) than in winter (43–46%) were still observed, indicating a more
576 significant role of secondary production in summer. The diurnal cycles of organics were
577 similar during all seasons, all characterized by two pronounced peaks. While the diurnal
578 cycles of secondary sulfate were overall relatively flat during most months of the year,
579 those of nitrate varied greatly in different seasons. It was evident that the diurnal cycles
580 of nitrate are driven by gas-particle partitioning and daytime photochemical production in
581 summer and winter, respectively. The winter season showed substantially different
582 concentrations of aerosol species between weekdays and weekends, with much lower
583 concentrations on weekends. However, no significant weekend effects were observed
584 during the other seasons.

585 Meteorological conditions play important roles in the formation of severe PM
586 pollution in Beijing. In this study, we illustrate the influences of RH and *T* on aerosol
587 loading and chemistry in different seasons. All aerosol species increased significantly
588 under stagnant meteorological conditions associated with high RH and low WS. NR-
589 PM₁ showed two high concentration regions ($> 60 \mu\text{g m}^{-3}$) at RH $> 60\%$. While organics
590 comprised a major fraction of NR-PM₁ in these two regions, the abundances of sulfate
591 and nitrate and air temperature were largely different, suggesting they play different roles
592 in causing PM pollution during different seasons. Under drier conditions (RH $< 30\%$), the
593 NR-PM₁ concentration was generally low and organics contributed more than 50% of its
594 mass, indicating the importance of organics during clean periods. The semi-volatile
595 nitrate presented the largest contribution under high RH and high *T*, highlighting the

596 importance of nitrate formation via aqueous-phase processing in summer. All NR-PM₁
597 species showed obvious dependence on wind direction, with higher concentrations
598 commonly associated with winds from the S, E and SE. This was consistent with the
599 results from PSCF analysis, which showed that the high potential source areas were
600 mainly located to the S and SW of Beijing. The high potential source areas varied
601 differently during the four seasons. A common high potential source area to the SW of
602 Beijing, along the Taihang Mountains, was observed during all seasons except winter,
603 demonstrating the potentially high impact of regional transport on severe PM pollution in
604 Beijing. The winter season showed a much smaller source region compared to the other
605 seasons, indicating that local and regional transport over a smaller regional scale are more
606 important. High potential source areas to the SE of Beijing were also observed for
607 organics, nitrate and chloride in summer, likely due to agricultural burning.

608

609 **Acknowledgements**

610 This work was supported by the National Key Project of Basic Research
611 (2014CB447900; 2013CB955801), the Strategic Priority Research Program (B) of the
612 Chinese Academy of Sciences (XDB05020501), and the National Natural Science
613 Foundation of China (41175108).

614

615 **References**

616 Budisulistiorini, S. H., Canagaratna, M. R., Croteau, P. L., Marth, W. J., Baumann, K.,
617 Edgerton, E. S., Shaw, S., Knipping, E. M., Worsnop, D. R., and Jayne, J. T.: Real-
618 time continuous characterization of secondary organic aerosol derived from isoprene
619 epoxydiols (IEPOX) in downtown Atlanta, Georgia, using the Aerodyne Aerosol
620 Chemical Speciation Monitor (ACSM), Environ. Sci. Technol., 47, 5686-5694, 2013.
621 Budisulistiorini, S. H., Canagaratna, M. R., Croteau, P. L., Baumann, K., Edgerton, E. S.,
622 Kollman, M. S., Ng, N. L., Verma, V., Shaw, S. L., Knipping, E. M., Worsnop, D. R.,
623 Jayne, J. T., Weber, R. J., and Surratt, J. D.: Intercomparison of an Aerosol Chemical
624 Speciation Monitor (ACSM) with ambient fine aerosol measurements in downtown
625 Atlanta, Georgia, Atmos. Meas. Tech., 7, 1929-1941, 10.5194/amt-7-1929-2014,
626 2014.

627 Canagaratna, M., Jayne, J., Jimenez, J. L., Allan, J. A., Alfarra, R., Zhang, Q., Onasch,
628 T., Drewnick, F., Coe, H., Middlebrook, A., Delia, A., Williams, L., Trimborn, A.,
629 Northway, M., Kolb, C., Davidovits, P., and Worsnop, D.: Chemical and
630 microphysical characterization of aerosols via Aerosol Mass Spectrometry, Mass
631 Spectrom. Rev., 26, 185-222, 2007.

632 Cao, J., Xu, H., Xu, Q., Chen, B., and Kan, H.: Fine particulate matter constituents and
633 cardiopulmonary mortality in a heavily polluted Chinese city, Environ. Health
634 Perspect., 120, 373 - 378, 2012.

635 Carbone, S., Saarikoski, S., Frey, A., Reyes, F., Reyes, P., Castillo, M., Gramsch, E.,
636 Oyola, P., Jayne, J., and Worsnop, D. R.: Chemical characterization of submicron
637 aerosol particles in Santiago de Chile, Aerosol Air Qual. Res., 13, 462-473, 2013.

638 Chen, Y., Sheng, G., Bi, X., Feng, Y., Mai, B., and Fu, J.: Emission factors for
639 carbonaceous particles and polycyclic aromatic hydrocarbons from residential coal
640 combustion in China, Environ. Sci. Technol., 39, 1861-1867, 10.1021/es0493650,
641 2005.

642 Cheng, Y., Engling, G., He, K.-B., Duan, F.-K., Du, Z.-Y., Ma, Y.-L., Liang, L.-L., Lu,
643 Z.-F., Liu, J.-M., Zheng, M., and Weber, R. J.: The characteristics of Beijing aerosol
644 during two distinct episodes: Impacts of biomass burning and fireworks, Environ.
645 Pollut., 185, 149-157, <http://dx.doi.org/10.1016/j.envpol.2013.10.037>, 2014.

646 DeCarlo, P. F., Kimmel, J. R., Trimborn, A., Northway, M. J., Jayne, J. T., Aiken, A. C.,
647 Gonin, M., Fuhrer, K., Horvath, T., Docherty, K. S., Worsnop, D. R., and Jimenez, J.
648 L.: Field-Deployable, High-Resolution, Time-of-Flight Aerosol Mass Spectrometer,
649 Anal. Chem., 78, 8281-8289, 2006.

650 Docherty, K. S., Aiken, A. C., Huffman, J. A., Ulbrich, I. M., DeCarlo, P. F., Sueper, D.,
651 Worsnop, D. R., Snyder, D. C., Peltier, R. E., Weber, R. J., Grover, B. D., Eatough,
652 D. J., Williams, B. J., Goldstein, A. H., Ziemann, P. J., and Jimenez, J. L.: The 2005
653 Study of Organic Aerosols at Riverside (SOAR-1): instrumental intercomparisons
654 and fine particle composition, Atmos. Chem. Phys., 11, 12387-12420, 10.5194/acp-
655 11-12387-2011, 2011.

656 Draxler, R. R., and Rolph, G. D.: HYSPLIT (HYbrid Single-Particle Lagrangian
657 Integrated Trajectory) Model access via NOAA ARL READY Website
658 (<http://www.arl.noaa.gov/ready/hysplit4.html>), NOAA Air Resources Laboratory,
659 Silver Spring, MD., 2003.

660 Drewnick, F., Hings, S. S., DeCarlo, P. F., Jayne, J. T., Gonin, M., Fuhrer, K., Weimer,
661 S., Jimenez, J. L., Demerjian, K. L., Borrmann, S., and Worsnop, D. R.: A new Time-
662 of-Flight Aerosol Mass Spectrometer (ToF-AMS) – Instrument description and first
663 field deployment., Aerosol Sci. Technol., 39, 637-658, 2005.

664 Gong, Z., Lan, Z., Xue, L., Zeng, L., He, L., and Huang, X.: Characterization of
665 submicron aerosols in the urban outflow of the central Pearl River Delta region of
666 China, Front. Environ. Sci. Eng., 6, 725-733, 10.1007/s11783-012-0441-8, 2012.

667 Guo, S., Hu, M., Zamora, M. L., Peng, J., Shang, D., Zheng, J., Du, Z., Wu, Z., Shao, M.,
668 Zeng, L., Molina, M. J., and Zhang, R.: Elucidating severe urban haze formation in
669 China, Proc. Natl. Acad. Sci. U.S.A., 111, 17373-17378, 10.1073/pnas.1419604111,
670 2014.

671 Han, S., Kondo, Y., Oshima, N., Takegawa, N., Miyazaki, Y., Hu, M., Lin, P., Deng, Z.,
672 Zhao, Y., Sugimoto, N., and Wu, Y.: Temporal variations of elemental carbon in
673 Beijing, *J. Geophys. Res.*, 114, D23202, doi:23210.21029/22009JD012027, 2009.

674 He, L.-Y., Huang, X.-F., Xue, L., Hu, M., Lin, Y., Zheng, J., Zhang, R., and Zhang, Y.-
675 H.: Submicron aerosol analysis and organic source apportionment in an urban
676 atmosphere in Pearl River Delta of China using high-resolution aerosol mass
677 spectrometry, *J. Geophys. Res.*, 116, D12304, 10.1029/2010jd014566, 2011.

678 Hu, M., Wu, Z., Slanina, J., Lin, P., Liu, S., and Zeng, L.: Acidic gases, ammonia and
679 water-soluble ions in PM_{2.5} at a coastal site in the Pearl River Delta, China, *Atmos.*
680 *Environ.*, 42, 6310-6320, 10.1016/j.atmosenv.2008.02.015, 2008.

681 Hu, W. W., Hu, M., Yuan, B., Jimenez, J. L., Tang, Q., Peng, J. F., Hu, W., Shao, M.,
682 Wang, M., Zeng, L. M., Wu, Y. S., Gong, Z. H., Huang, X. F., and He, L. Y.: Insights
683 on organic aerosol aging and the influence of coal combustion at a regional receptor
684 site of central eastern China, *Atmos. Chem. Phys.*, 13, 10095-10112, 10.5194/acp-13-
685 10095-2013, 2013.

686 Huang, R.-J., Zhang, Y., Bozzetti, C., Ho, K.-F., Cao, J.-J., Han, Y., Daellenbach, K. R.,
687 Slowik, J. G., Platt, S. M., Canonaco, F., Zotter, P., Wolf, R., Pieber, S. M., Bruns, E.
688 A., Crippa, M., Ciarelli, G., Piazzalunga, A., Schwikowski, M., Abbaszade, G.,
689 Schnelle-Kreis, J., Zimmermann, R., An, Z., Szidat, S., Baltensperger, U., Haddad, I.
690 E., and Prevot, A. S. H.: High secondary aerosol contribution to particulate pollution
691 during haze events in China, *Nature*, 514, 218 - 222, 10.1038/nature13774, 2014.

692 Huang, X. F., He, L. Y., Hu, M., Canagaratna, M. R., Sun, Y., Zhang, Q., Zhu, T., Xue,
693 L., Zeng, L. W., Liu, X. G., Zhang, Y. H., Jayne, J. T., Ng, N. L., and Worsnop, D.
694 R.: Highly time-resolved chemical characterization of atmospheric submicron
695 particles during 2008 Beijing Olympic Games using an Aerodyne High-Resolution
696 Aerosol Mass Spectrometer, *Atmos. Chem. Phys.*, 10, 8933-8945, 10.5194/acp-10-
697 8933-2010, 2010.

698 Huang, X. F., He, L. Y., Hu, M., Canagaratna, M. R., Kroll, J. H., Ng, N. L., Zhang, Y.
699 H., Lin, Y., Xue, L., Sun, T. L., Liu, X. G., Shao, M., Jayne, J. T., and Worsnop, D.
700 R.: Characterization of submicron aerosols at a rural site in Pearl River Delta of
701 China using an Aerodyne High-Resolution Aerosol Mass Spectrometer, *Atmos.*
702 *Chem. Phys.*, 11, 1865-1877, 10.5194/acp-11-1865-2011, 2011.

703 Huang, X. F., He, L. Y., Xue, L., Sun, T. L., Zeng, L. W., Gong, Z. H., Hu, M., and Zhu,
704 T.: Highly time-resolved chemical characterization of atmospheric fine particles
705 during 2010 Shanghai World Expo, *Atmos. Chem. Phys.*, 12, 4897-4907,
706 10.5194/acp-12-4897-2012, 2012.

707 Huang, X.-F., Xue, L., Tian, X.-D., Shao, W.-W., Sun, T.-L., Gong, Z.-H., Ju, W.-W.,
708 Jiang, B., Hu, M., and He, L.-Y.: Highly time-resolved carbonaceous aerosol
709 characterization in Yangtze River Delta of China: composition, mixing state and
710 secondary formation, *Atmos. Environ.*, 64, 200 - 207,
711 10.1016/j.atmosenv.2012.09.059, 2013.

712 Huffman, J. A., Jayne, J. T., Drewnick, F., Aiken, A. C., Onasch, T., Worsnop, D. R., and
713 Jimenez, J. L.: Design, modeling, optimization, and experimental tests of a particle
714 beam width probe for the Aerodyne Aerosol Mass Spectrometer, *Aerosol Sci.*
715 *Technol.*, 39, 1143-1163, 2005.

716 Huffman, J. A., Docherty, K. S., Aiken, A. C., Cubison, M. J., Ulbrich, I. M., DeCarlo, P.
717 F., Sueper, D., Jayne, J. T., Worsnop, D. R., Ziemann, P. J., and Jimenez, J. L.:
718 Chemically-resolved aerosol volatility measurements from two megacity field
719 studies, *Atmos. Chem. Phys.*, 9, 7161-7182, 2009.

720 Ianniello, A., Spataro, F., Esposito, G., Allegrini, I., Rantica, E., Ancora, M. P., Hu, M.,
721 and Zhu, T.: Occurrence of gas phase ammonia in the area of Beijing (China), *Atmos.*
722 *Chem. Phys.*, 10, 9487-9503, 10.5194/acp-10-9487-2010, 2010.

723 Jayne, J. T., Leard, D. C., Zhang, X., Davidovits, P., Smith, K. A., Kolb, C. E., and
724 Worsnop, D. R.: Development of an aerosol mass spectrometer for size and
725 composition analysis of submicron particles, *Aerosol Sci. Technol.*, 33, 49-70, 2000.

726 Ji, D., Li, L., Wang, Y., Zhang, J., Cheng, M., Sun, Y., Liu, Z., Wang, L., Tang, G., Hu,
727 B., Chao, N., Wen, T., and Miao, H.: The heaviest particulate air-pollution episodes
728 occurred in northern China in January, 2013: Insights gained from observation,
729 *Atmos. Environ.*, 92, 546-556, <http://dx.doi.org/10.1016/j.atmosenv.2014.04.048>,
730 2014.

731 Liu, Q.: Physical and chemical characteristics of submicron aerosol and its sources in
732 Beijing, LAPC, Institute of Atmospheric Physics, Chinese Academy of Sciences,
733 2012.

734 Matthew, B. M., Middlebrook, A. M., and Onasch, T. B.: Collection efficiencies in an
735 Aerodyne Aerosol Mass Spectrometer as a function of particle phase for paboratory
736 generated aerosols, *Aerosol Sci. Technol.*, 42, 884 - 898, 2008.

737 Meng, Z. Y., Lin, W. L., Jiang, X. M., Yan, P., Wang, Y., Zhang, Y. M., Jia, X. F., and
738 Yu, X. L.: Characteristics of atmospheric ammonia over Beijing, China, *Atmos.*
739 *Chem. Phys.*, 11, 6139-6151, 10.5194/acp-11-6139-2011, 2011.

740 Middlebrook, A. M., Bahreini, R., Jimenez, J. L., and Canagaratna, M. R.: Evaluation of
741 composition-dependent collection efficiencies for the Aerodyne Aerosol Mass
742 Spectrometer using field data, *Aerosol Sci. Technol.*, 46, 258-271, 2012.

743 Ng, N. L., Herndon, S. C., Trimborn, A., Canagaratna, M. R., Croteau, P. L., Onasch, T.
744 B., Sueper, D., Worsnop, D. R., Zhang, Q., Sun, Y. L., and Jayne, J. T.: An Aerosol
745 Chemical Speciation Monitor (ACSM) for routine monitoring of the composition and
746 mass concentrations of ambient aerosol, *Aerosol Sci. Technol.*, 45, 770 - 784, 2011.

747 Parworth, C., Fast, J., Mei, F., Shippert, T., Sivaraman, C., Tilp, A., Watson, T., and
748 Zhang, Q.: Long-term Measurements of Submicrometer Aerosol Chemistry at the
749 Southern Great Plains (SGP) Using an Aerosol Chemical Speciation Monitor
750 (ACSM), *Atmos. Environ.*, 106, 43-55,
751 <http://dx.doi.org/10.1016/j.atmosenv.2015.01.060>, 2015.

752 Petit, J. E., Favez, O., Sciare, J., Crenn, V., Sarda-Esteve, R., Bonnaire, N., Močnik, G.,
753 Dupont, J. C., Haeffelin, M., and Leoz-Garziandia, E.: Two years of near real-time
754 chemical composition of submicron aerosols in the region of Paris using an Aerosol
755 Chemical Speciation Monitor (ACSM) and a multi-wavelength Aethalometer, *Atmos.*
756 *Chem. Phys.*, 15, 2985-3005, 10.5194/acp-15-2985-2015, 2015.

757 Polissar, A. V., P.K. Hopke, P. Paatero, Y.J. Kaufman, D.K. Hall, B.A. Bodhaine, E.G.
758 Dutton, J.M. Harris: The aerosol at Barrow, Alaska: long-term trends and source
759 locations, *Atmos. Environ.*, 33, 2441-2458, 1999.

760 Sun, J., Zhang, Q., Canagaratna, M. R., Zhang, Y., Ng, N. L., Sun, Y., Jayne, J. T.,
761 Zhang, X., Zhang, X., and Worsnop, D. R.: Highly time- and size-resolved

762 characterization of submicron aerosol particles in Beijing using an Aerodyne Aerosol
763 Mass Spectrometer, *Atmos. Environ.*, 44, 131-140, 2010.

764 Sun, Y. L., Wang, Z., Dong, H., Yang, T., Li, J., Pan, X., Chen, P., and Jayne, J. T.:
765 Characterization of summer organic and inorganic aerosols in Beijing, China with an
766 Aerosol Chemical Speciation Monitor, *Atmos. Environ.*, 51, 250-259,
767 10.1016/j.atmosenv.2012.01.013, 2012.

768 Sun, Y. L., Wang, Z., Fu, P., Jiang, Q., Yang, T., Li, J., and Ge, X.: The impact of
769 relative humidity on aerosol composition and evolution processes during wintertime
770 in Beijing, China, *Atmos. Environ.*, 77, 927-934,
771 <http://dx.doi.org/10.1016/j.atmosenv.2013.06.019>, 2013a.

772 Sun, Y. L., Wang, Z. F., Fu, P. Q., Yang, T., Jiang, Q., Dong, H. B., Li, J., and Jia, J. J.:
773 Aerosol composition, sources and processes during wintertime in Beijing, China,
774 *Atmos. Chem. Phys.*, 13, 4577-4592, 10.5194/acp-13-4577-2013, 2013b.

775 Sun, Y. L., Jiang, Q., Wang, Z., Fu, P., Li, J., Yang, T., and Yin, Y.: Investigation of the
776 sources and evolution processes of severe haze pollution in Beijing in January 2013,
777 *J. Geophys. Res.*, 119, 4380-4398, 10.1002/2014JD021641, 2014.

778 Viana, M., López, J. M., Querol, X., Alastuey, A., García-Gacio, D., Blanco-Heras, G.,
779 López-Mahía, P., Piñeiro-Iglesias, M., Sanz, M. J., Sanz, F., Chi, X., and Maenhaut,
780 W.: Tracers and impact of open burning of rice straw residues on PM in Eastern
781 Spain, *Atmos. Environ.*, 42, 1941-1957,
782 <http://dx.doi.org/10.1016/j.atmosenv.2007.11.012>, 2008.

783 Wang, L. T., Wei, Z., Yang, J., Zhang, Y., Zhang, F. F., Su, J., Meng, C. C., and Zhang,
784 Q.: The 2013 severe haze over southern Hebei, China: model evaluation, source
785 apportionment, and policy implications, *Atmos. Chem. Phys.*, 14, 3151-3173,
786 10.5194/acp-14-3151-2014, 2014a.

787 Wang, S. X., Zhao, B., Cai, S. Y., Klimont, Z., Nielsen, C. P., Morikawa, T., Woo, J. H.,
788 Kim, Y., Fu, X., Xu, J. Y., Hao, J. M., and He, K. B.: Emission trends and mitigation
789 options for air pollutants in East Asia, *Atmos. Chem. Phys.*, 14, 6571-6603,
790 10.5194/acp-14-6571-2014, 2014b.

791 Wang, Y., Zhang, Q. Q., He, K., Zhang, Q., and Chai, L.: Sulfate-nitrate-ammonium
792 aerosols over China: response to 2000–2015 emission changes of sulfur dioxide,
793 nitrogen oxides, and ammonia, *Atmos. Chem. Phys.*, 13, 2635-2652, 10.5194/acp-13-
794 2635-2013, 2013.

795 Wang, Z., Li, J., Wang, Z., Yang, W., Tang, X., Ge, B., Yan, P., Zhu, L., Chen, X., Chen,
796 H., Wang, W., Li, J., Liu, B., Wang, X., Wand, W., Zhao, Y., Lu, N., and Su, D.:
797 Modeling study of regional severe hazes over mid-eastern China in January 2013 and
798 its implications on pollution prevention and control, *Sci. China Earth Sci.*, 57, 3-13,
799 10.1007/s11430-013-4793-0, 2014c.

800 Xu, J., Zhang, Q., Chen, M., Ge, X., Ren, J., and Qin, D.: Chemical composition, sources,
801 and processes of urban aerosols during summertime in northwest China: insights from
802 high-resolution aerosol mass spectrometry, *Atmos. Chem. Phys.*, 14, 12593-12611,
803 10.5194/acp-14-12593-2014, 2014a.

804 Xu, W. Y., Zhao, C. S., Ran, L., Lin, W. L., Yan, P., and Xu, X. B.: SO₂ noontime-peak
805 phenomenon in the North China Plain, *Atmos. Chem. Phys.*, 14, 7757-7768,
806 10.5194/acp-14-7757-2014, 2014b.

807 Yang, F., Huang, L., Duan, F., Zhang, W., He, K., Ma, Y., Brook, J. R., Tan, J., Zhao, Q.,
808 and Cheng, Y.: Carbonaceous species in PM_{2.5} at a pair of rural/urban sites in Beijing,
809 2005–2008, *Atmos. Chem. Phys.*, 11, 7893-7903, 10.5194/acp-11-7893-2011, 2011.

810 Zhang, H., Wang, S., Hao, J., Wan, L., Jiang, J., Zhang, M., Mestl, H. E. S., Alnes, L. W.
811 H., Aunan, K., and Mellouki, A. W.: Chemical and size characterization of particles
812 emitted from the burning of coal and wood in rural households in Guizhou, China,
813 *Atmos. Environ.*, 51, 94-99, 10.1016/j.atmosenv.2012.01.042, 2012.

814 Zhang, Q., Jimenez, J. L., Worsnop, D. R., and Canagaratna, M.: A case study of urban
815 particle acidity and its effect on secondary organic aerosol, *Environ. Sci. Technol.*,
816 41, 3213-3219, 2007.

817 Zhang, R., Jing, J., Tao, J., Hsu, S. C., Wang, G., Cao, J., Lee, C. S. L., Zhu, L., Chen, Z.,
818 Zhao, Y., and Shen, Z.: Chemical characterization and source apportionment of PM_{2.5}
819 in Beijing: seasonal perspective, *Atmos. Chem. Phys.*, 13, 7053-7074, 10.5194/acp-
820 13-7053-2013, 2013a.

821 Zhang, Y., Schauer, J. J., Zhang, Y., Zeng, L., Wei, Y., Liu, Y., and Shao, M.:
822 Characteristics of particulate carbon emissions from real-world Chinese coal
823 combustion, *Environ. Sci. Technol.*, 42, 5068-5073, 2008.

824 Zhang, Y., Sun, J., Zhang, X., Shen, X., Wang, T., and Qin, M.: Seasonal
825 characterization of components and size distributions for submicron aerosols in
826 Beijing, *Sci. China Earth Sci.*, 56, 890 - 900, 10.1007/s11430-012-4515-z, 2013b.

827 Zhang, Y. J., Tang, L. L., Wang, Z., Yu, H. X., Sun, Y. L., Liu, D., Qin, W., Canonaco,
828 F., Prévôt, A. S. H., Zhang, H. L., and Zhou, H. C.: Insights into characteristics,
829 sources, and evolution of submicron aerosols during harvest seasons in the Yangtze
830 River delta region, China, *Atmos. Chem. Phys.*, 15, 1331-1349, 10.5194/acp-15-
831 1331-2015, 2015.

832 Zhao, P. S., Dong, F., He, D., Zhao, X. J., Zhang, X. L., Zhang, W. Z., Yao, Q., and Liu,
833 H. Y.: Characteristics of concentrations and chemical compositions for PM_{2.5} in the
834 region of Beijing, Tianjin, and Hebei, China, *Atmos. Chem. Phys.*, 13, 4631-4644,
835 10.5194/acp-13-4631-2013, 2013.

836 Zhao, X., Zhang, X., Xu, X., Xu, J., Meng, W., and Pu, W.: Seasonal and diurnal
837 variations of ambient PM_{2.5} concentration in urban and rural environments in Beijing,
838 *Atmos. Environ.*, 43, 2893-2900, 2009.

839 Zheng, G. J., Duan, F. K., Su, H., Ma, Y. L., Cheng, Y., Zheng, B., Zhang, Q., Huang, T.,
840 Kimoto, T., Chang, D., Pöschl, U., Cheng, Y. F., and He, K. B.: Exploring the severe
841 winter haze in Beijing: the impact of synoptic weather, regional transport and
842 heterogeneous reactions, *Atmos. Chem. Phys.*, 15, 2969-2983, 10.5194/acp-15-2969-
843 2015, 2015.

844 Zheng, M., Salmon, L. G., Schauer, J. J., Zeng, L., Kiang, C. S., Zhang, Y., and Cass, G.
845 R.: Seasonal trends in PM_{2.5} source contributions in Beijing, China, *Atmos. Environ.*,
846 39, 3967-3976, DOI: 10.1016/j.atmosenv.2005.03.036, 2005.

847 **Tables**

848 **Table 1.** Summary of mass concentrations of NR-PM₁ species, gaseous pollutants and
 849 meteorological parameters during the four seasons and entire study period.

	Entire study		Summer		Fall		Winter		Spring	
	mean	s.d.	mean	s.d.	mean	s.d.	mean	s.d.	mean	s.d.
Org (µg m ⁻³)	25.7	22.1	24.5	20.7	26.8	24.7	29.6	24.8	21.7	16.0
SO ₄ ²⁻ (µg m ⁻³)	8.1	8.3	10.6	8.2	6.5	7.5	7.7	9.2	7.3	7.6
NO ₃ ⁻ (µg m ⁻³)	12.6	12.8	15.6	14.4	11.4	12.7	10.3	9.5	13.1	13.4
NH ₄ ⁺ (µg m ⁻³)	8.5	7.9	10.2	8.2	6.9	7.3	8.1	7.4	8.8	8.1
Cl ⁻ (µg m ⁻³)	1.8	2.5	0.8	1.5	1.7	2.7	3.0	3.0	1.5	1.9
NR-PM ₁ (µg m ⁻³)	56.6	48.2	61.6	48.8	53.3	49.7	58.7	50.5	52.3	42.7
SO ₂ (ppb)	16.2	14.0	5.4	0.8			25.3	16.0	11.5	8.3
CO (ppm)	1.5	1.3	1.8	1.3			1.7	1.6	1.2	1.0
NO (ppb)	30.0	43.0	7.8	10.8	41.9	51.2	50.9	50.9	19.8	30.0
NO _y (ppb)	64.0	55.5	35.6	17.9	77.8	63.1	89.1	66.6	54.0	43.3
O ₃ (ppb)	21.2	23.8	33.3	29.1	20.3	24.4	7.9	8.5	20.8	19.3
RH (%)	47.0	23.4	62.7	18.9	52.7	20.0	35.6	20.3	36.5	22.5
T (°C)	13.3	11.6	26.3	3.6	14.1	7.0	-1.3	3.4	14.6	8.4
WS, 8 m (m s ⁻¹)	1.2	0.8	1.0	0.5	0.9	0.7	1.4	1.0	1.4	0.9
WS, 240 m (m s ⁻¹)	4.4	3.0	3.5	2.3	4.1	2.7	4.6	3.4	5.3	3.3

850

851 **Figure captions:**

852 Fig. 1. (a) Map of the sampling site (IAP). (b) Wind rose plots, color coded by wind
853 speed (m s^{-1}) for each season. The frequencies are set to the same scales for all seasons.

854 Fig. 2. Monthly variation of (a) gaseous O_3 and NO_y , (b) precipitation (Precip.) and solar
855 radiation (SR), (c) wind speed (WS) and pressure (P), and (d) relative humidity (RH) and
856 temperature (T). The WS at the heights of 8 m (solid gray circles) and 240 m (solid black
857 circles) are shown in (c).

858 Fig. 3. Time series of NR- PM_1 species for the entire year. The pie charts show the
859 average chemical composition of NR- PM_1 during the four seasons (summer, fall, winter
860 and spring).

861 Fig. 4. Frequency of NR- PM_1 mass loadings during the four seasons: (a) summer; (b) fall;
862 (c) winter; (d) spring. Note that the frequency was calculated with 15 min average data.

863 Fig. 5. Seasonal variation of non-refractory submicron aerosol species. The bars represent
864 the 25th and 75th percentiles, and the solid circles are mean values.

865 Fig. 6. Monthly variation of (a) mass concentrations and (b) mass fractions of NR- PM_1
866 species.

867 Fig. 7. Monthly average diurnal cycle of (a) organics, (b) sulfate, (c) nitrate, and (d)
868 chloride during the four seasons.

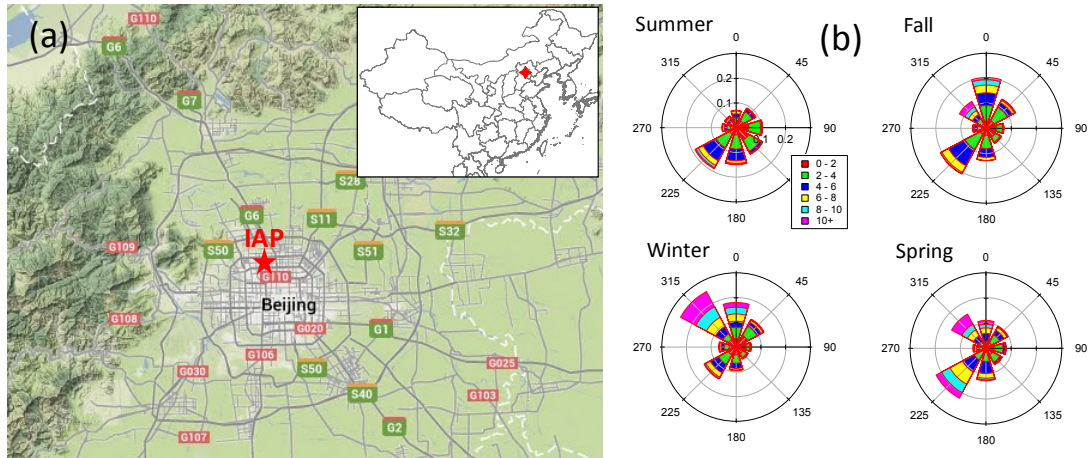
869 Fig. 8. Comparison of the average diurnal cycles of (a) organics, (b) SO_4^{2-} , (c) NO_3^- , and
870 (d) Cl^- between weekdays and weekends during the four seasons. Note that the periods
871 with $\text{NR-PM}_1 < 20 \mu\text{g m}^{-3}$ are excluded.

872 Fig. 9. RH/ T dependence of (a) NR- PM_1 mass concentration and (b) WS for a whole
873 year. The data are grouped into grids with increments of RH and T being 5% and 3°C,
874 respectively. Grid cells with the number of data points fewer than 10 are excluded.

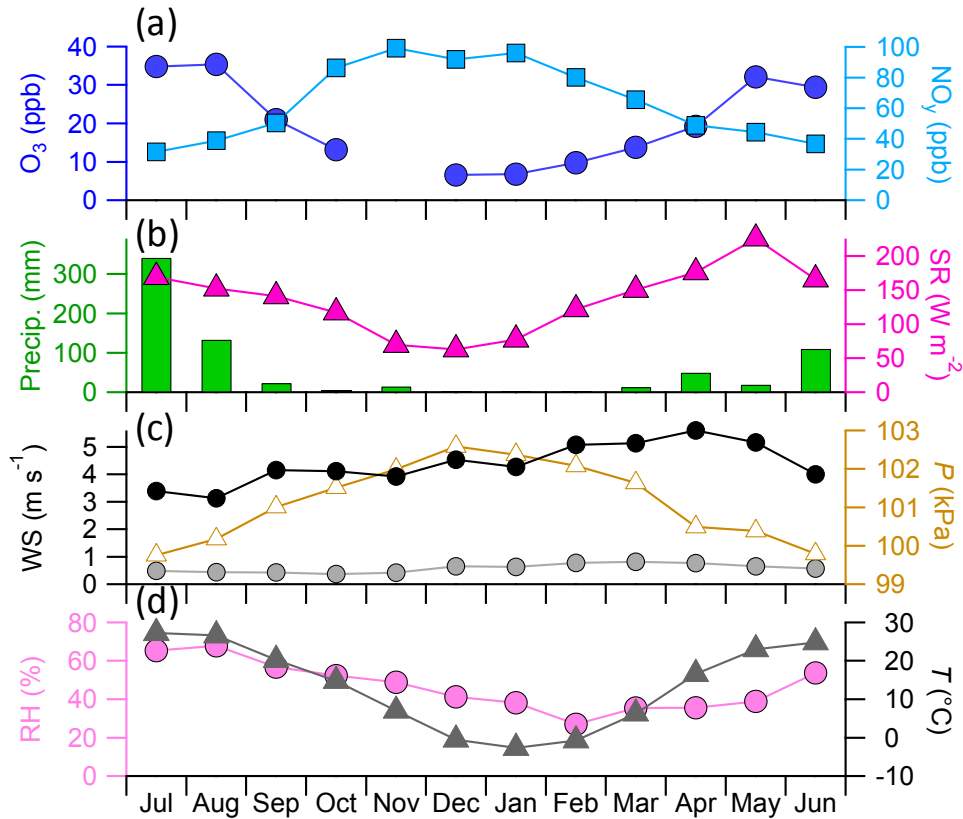
875 Fig. 10. RH/ T dependence of mass concentrations and mass fractions of aerosol species
876 for a whole year: (a) organics; (b) sulfate; (c) nitrate; (d) chloride. The data are grouped
877 into grids with increments of RH and T being 5% and 3°C, respectively. Grid cells with
878 the number of data points fewer than 10 are excluded.

879 Fig. 11. Box plots of mass concentrations of (a) organics, (b) SO_4^{2-} , (c) NO_3^- , and (d) Cl^-
880 as a function of wind directions sectors. All the data were segregated into eight wind
881 sectors representing north (N), northeast (NE), east (E), southeast (SE), south (S),
882 southwest (SW), west (W), and northwest (NW). The mean (cross), median (horizontal
883 line), 25th and 75th percentiles (lower and upper box), and 10th and 90th percentiles
884 (lower and upper whiskers) are shown.

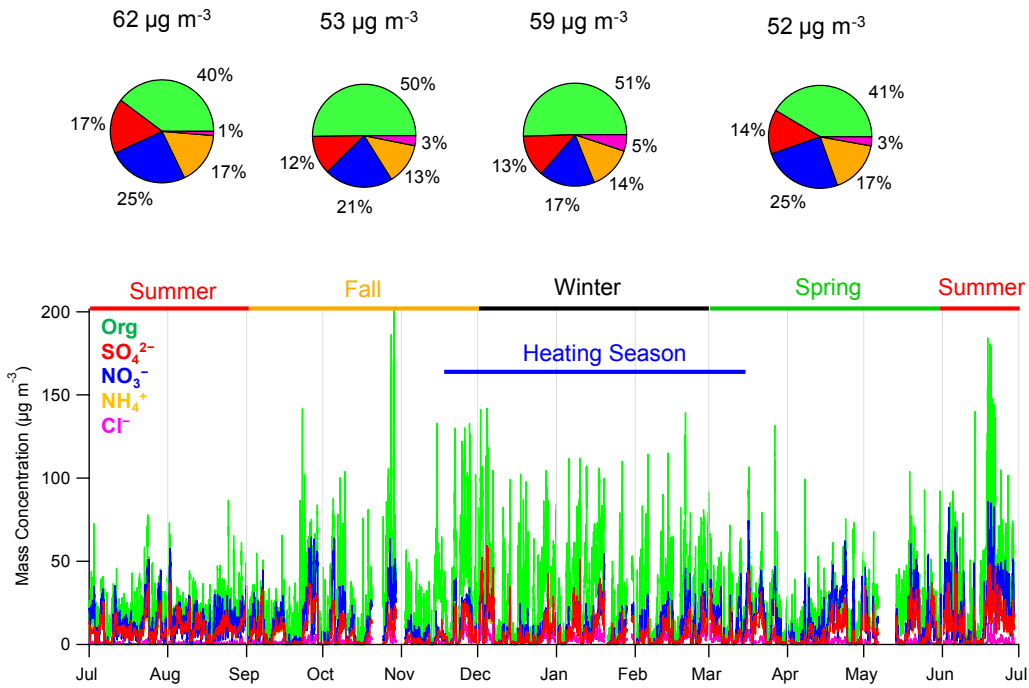
885 Fig. 12. PSCF of NR- PM_1 species during four seasons: (a) organics; (b) sulfate; (c)
886 nitrate; (d) chloride. The cities marked in each panel are Beijing (BJ), Tianjing (TJ),
887 Langfang (LF), Baoding (BD), Shijiazhuang (SJZ), and Hengshui (HS). The color scales
888 indicate the values of PSCF.



890 Fig. 1. (a) Map of the sampling site (IAP). (b) Wind rose plots, color coded by wind
891 speed (m s^{-1}) for each season. The frequencies are set to the same scales for all seasons.

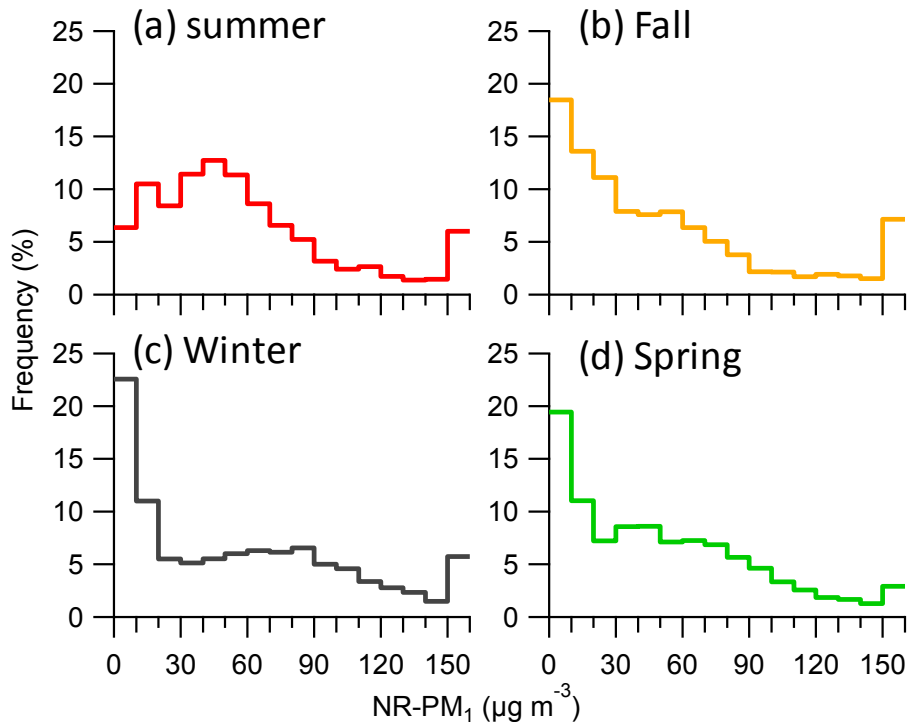


893 Fig. 2. Monthly variation of (a) gaseous O₃ and NO_y, (b) precipitation (Precip.) and solar
894 radiation (SR), (c) wind speed (WS) and pressure (P), and (d) relative humidity (RH) and
895 temperature (T). The WS at the heights of 8 m (solid gray circles) and 240 m (solid black
896 circles) are shown in (c).



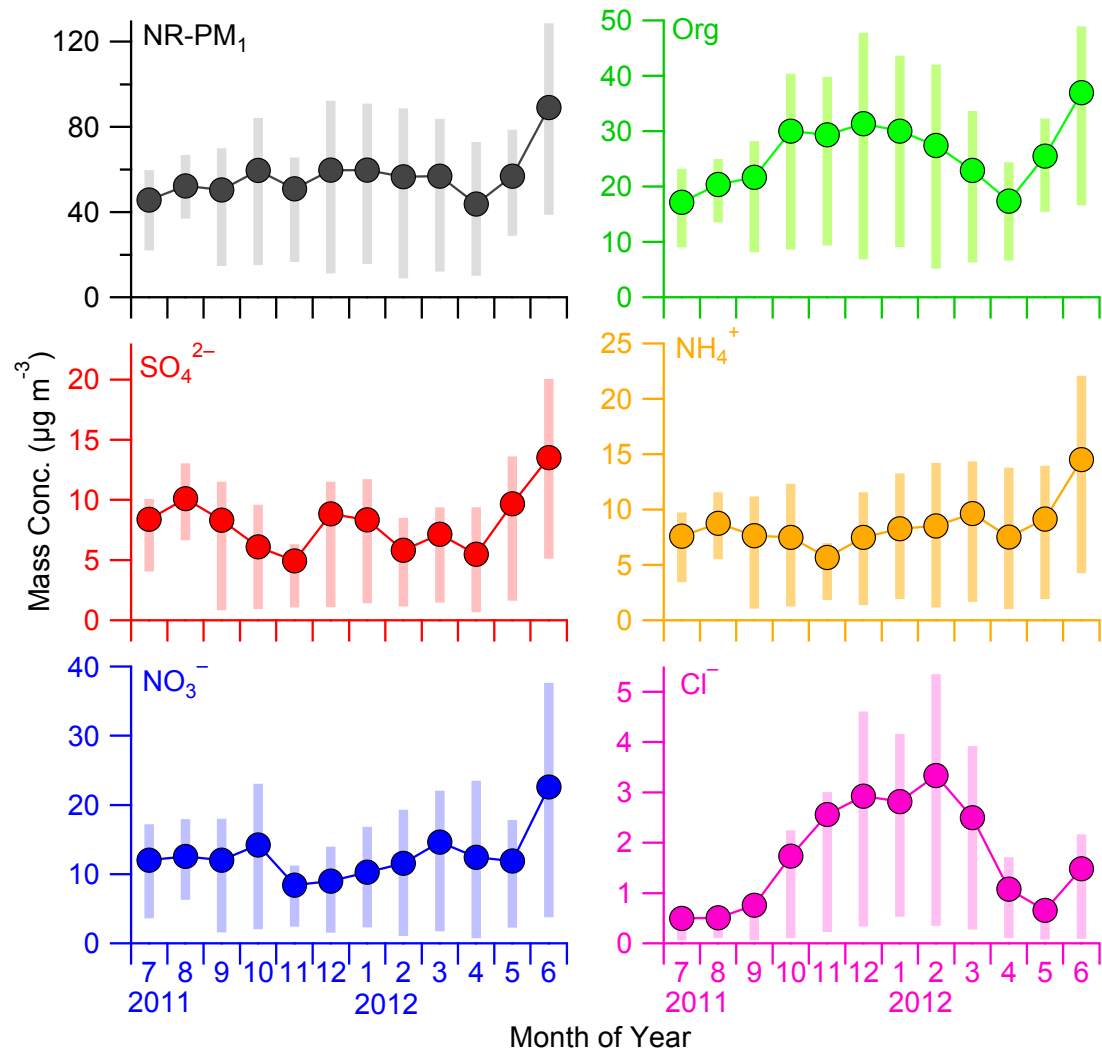
897

898 Fig. 3. Time series of NR-PM₁ species for the entire year. The pie charts show the
 899 average chemical composition of NR-PM₁ during the four seasons (summer, fall, winter
 900 and spring).



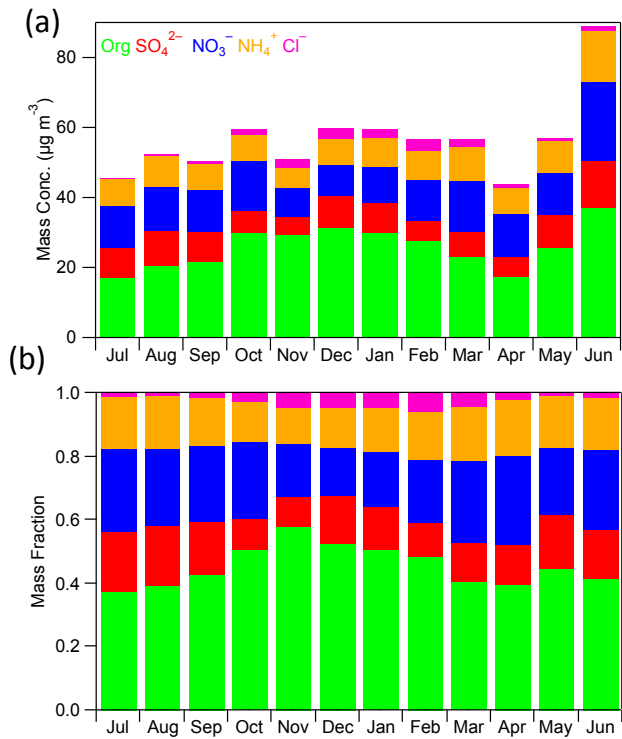
901

902 Fig. 4. Frequency of NR-PM₁ mass loadings during the four seasons: (a) summer; (b) fall;
 903 (c) winter; (d) spring. Note that the frequency was calculated with 15 min average data.



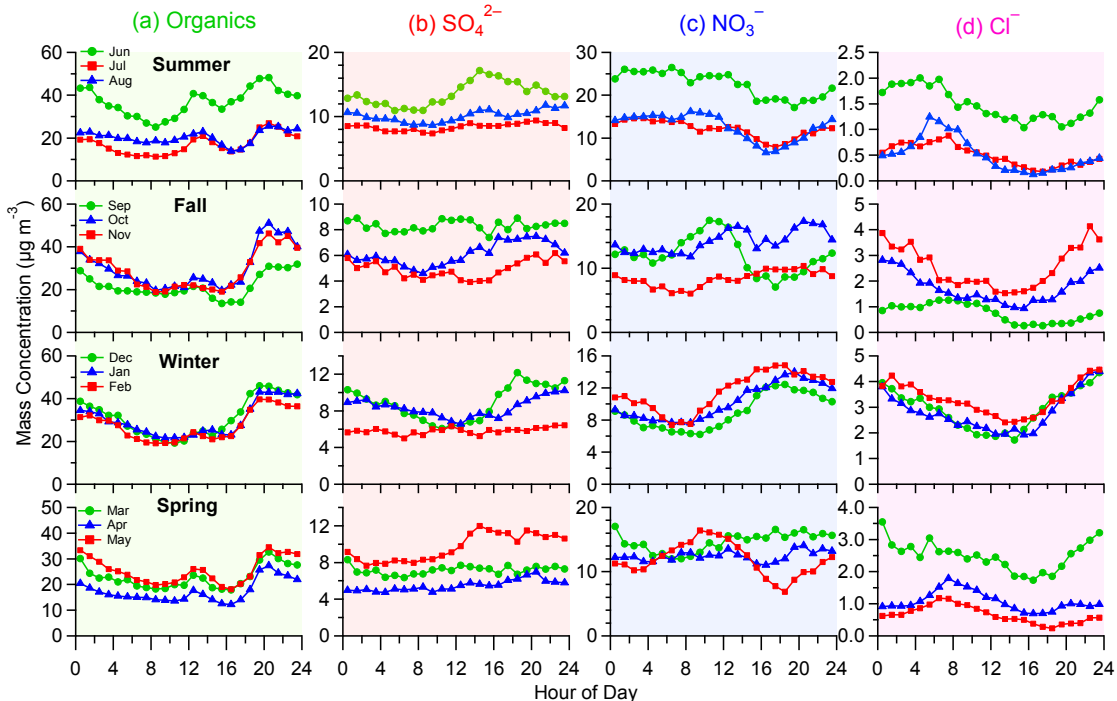
904
905

906 Fig. 5. Seasonal variation of non-refractory submicron aerosol species. The bars represent
907 the 25th and 75th percentiles, and the solid circles are mean values.



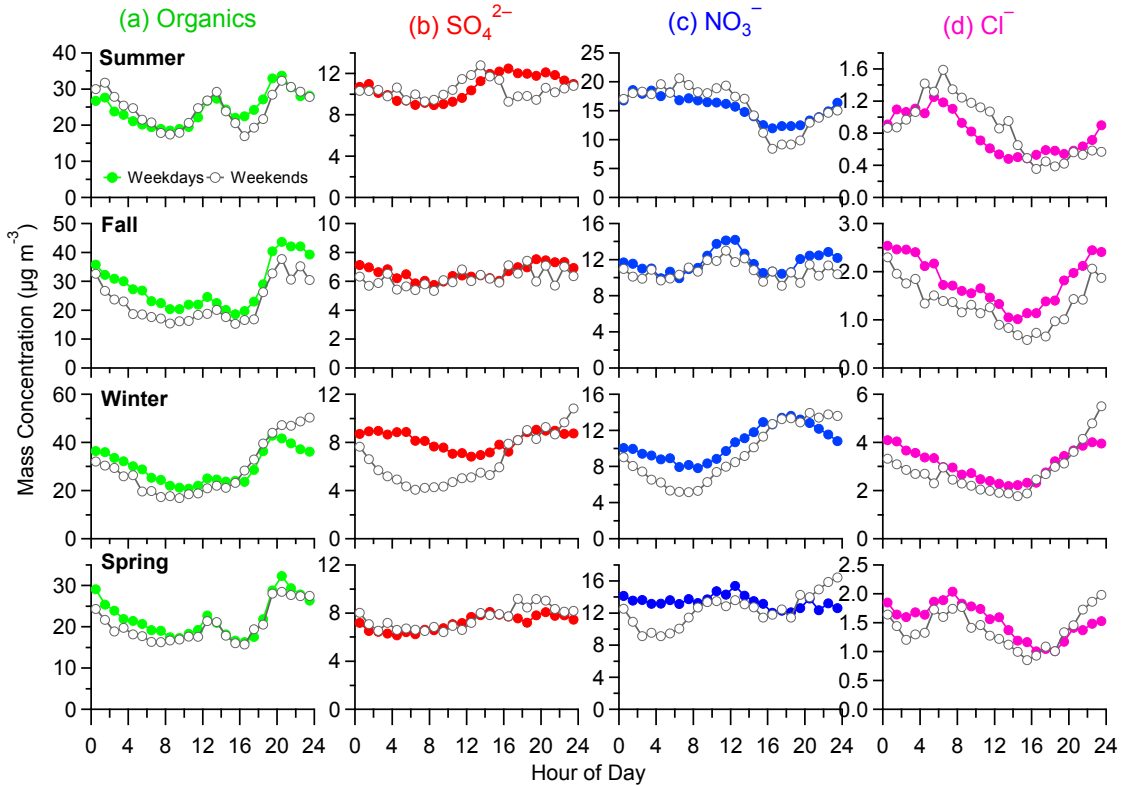
908

909 Fig. 6. Monthly variation of (a) mass concentrations and (b) mass fractions of NR-PM₁
 910 species.

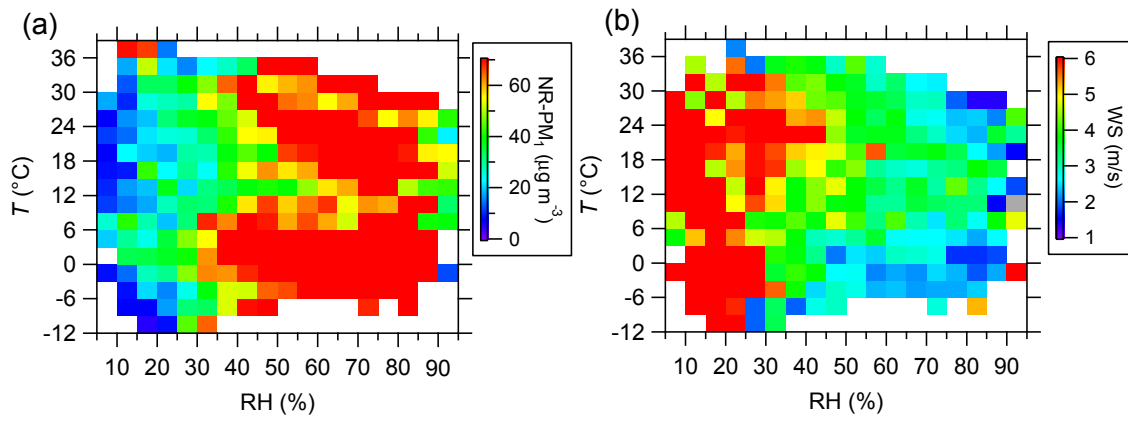


911

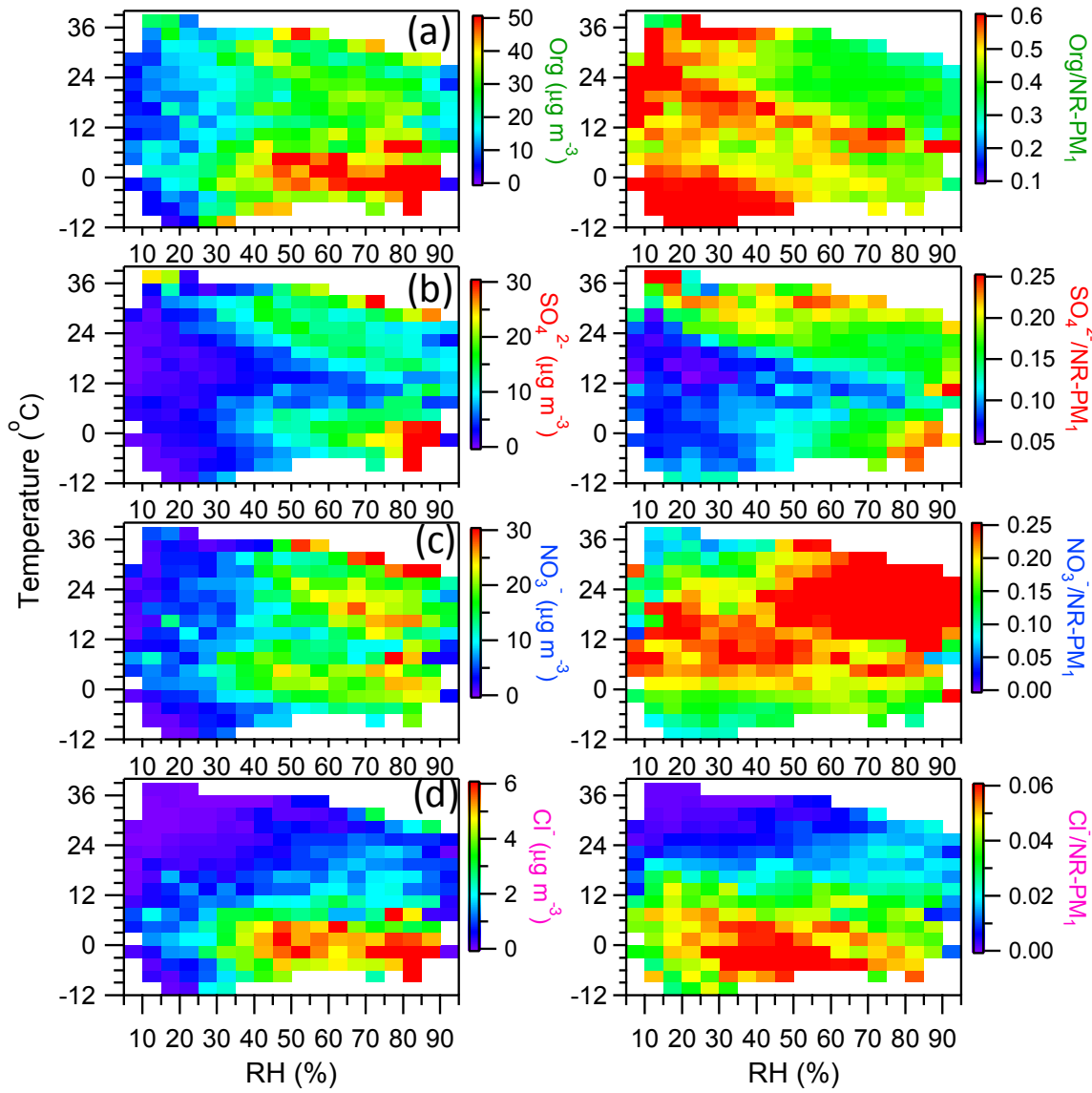
912 Fig. 7. Monthly average diurnal cycle of (a) organics, (b) sulfate, (c) nitrate, and (d)
 913 chloride during the four seasons.



914
915 Fig. 8. Comparison of the average diurnal cycles of (a) organics, (b) SO_4^{2-} , (c) NO_3^- , and
916 (d) Cl^- between weekdays and weekends during the four seasons. Note that the periods
917 with $\text{NR-PM}_1 < 20 \mu\text{g m}^{-3}$ are excluded.
918



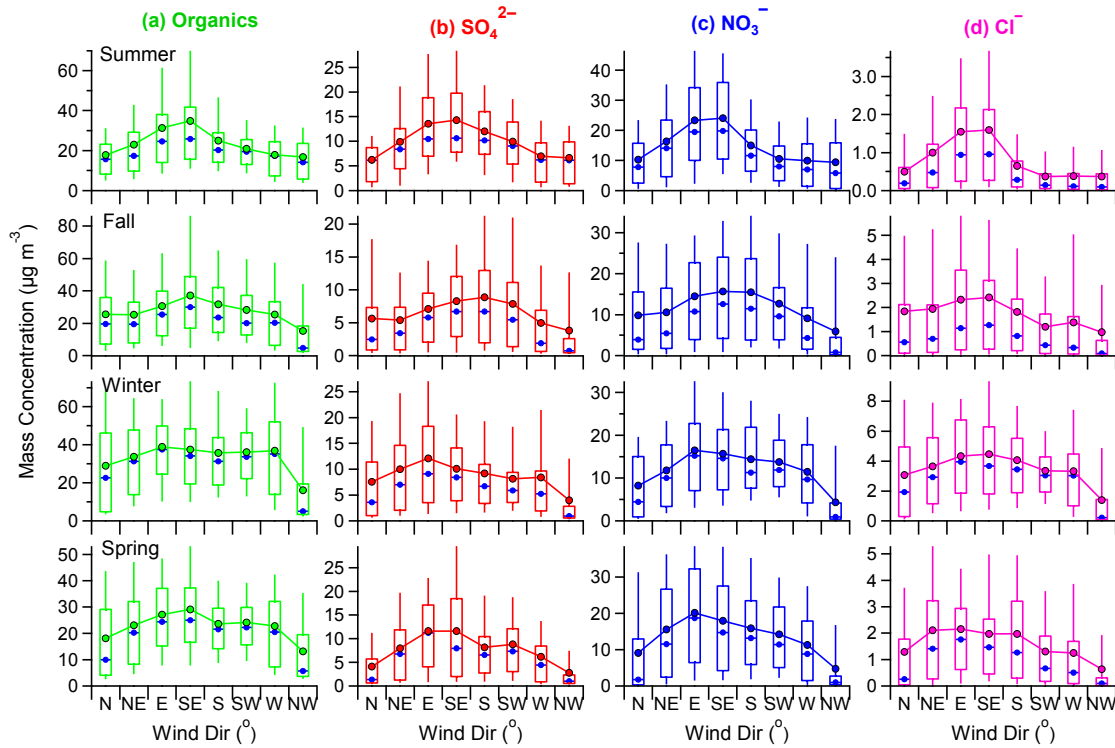
919
920 Fig. 9. RH/T dependence of (a) NR-PM₁ mass concentration and (b) WS for a whole
921 year. The data are grouped into grids with increments of RH and T being 5% and 3°C,
922 respectively. Grid cells with the number of data points fewer than 10 are excluded.



923

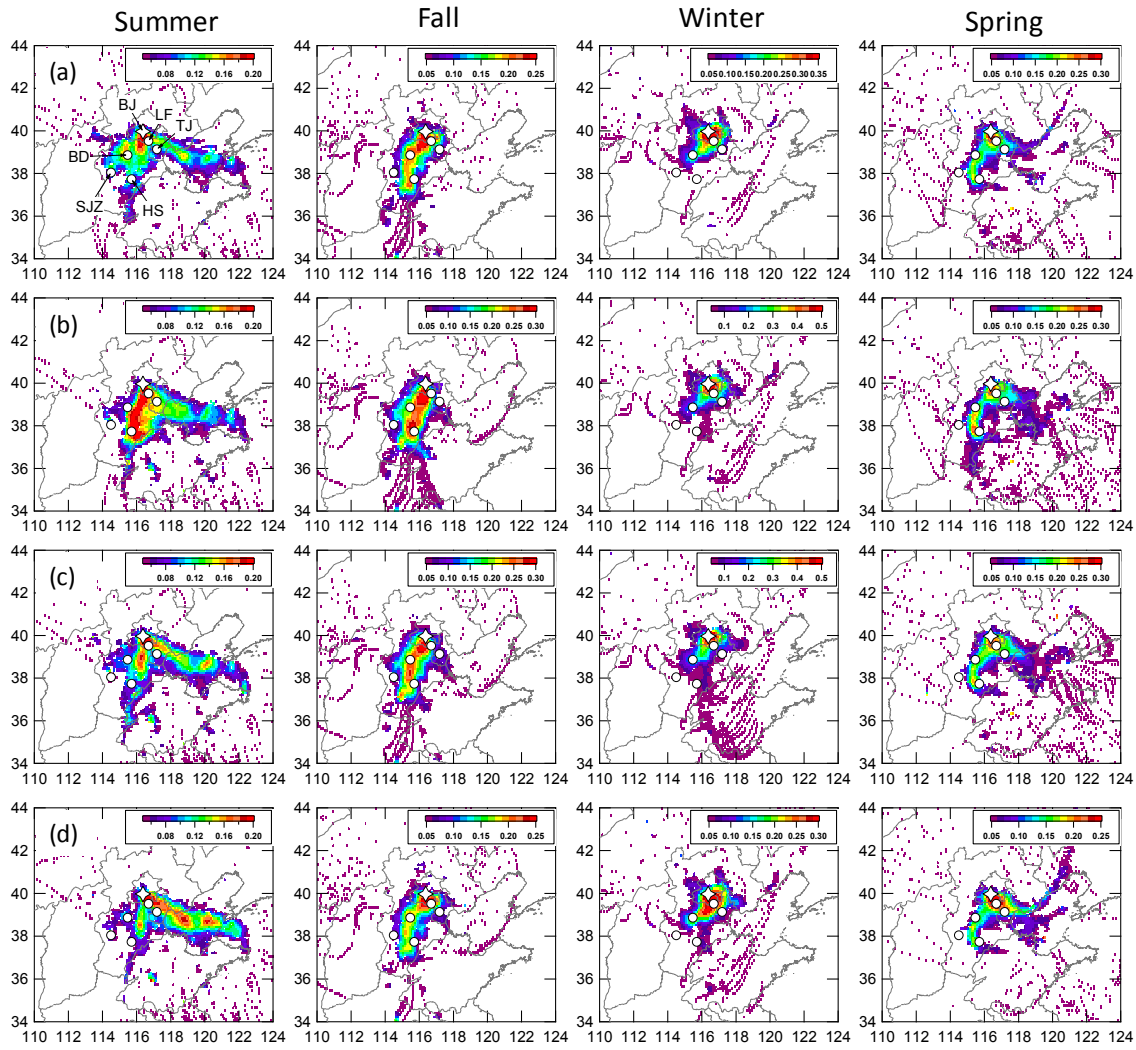
924

925 Fig. 10. RH/T dependence of mass concentrations and mass fractions of aerosol species
 926 for a whole year: (a) organics; (b) sulfate; (c) nitrate; (d) chloride. The data are grouped
 927 into grids with increments of RH and T being 5% and 3°C, respectively. Grid cells with
 the number of data points fewer than 10 are excluded.



928

929 Fig. 11. Box plots of mass concentrations of (a) organics, (b) SO_4^{2-} , (c) NO_3^- , and (d) Cl^-
 930 as a function of wind directions sectors. All the data were segregated into eight wind
 931 sectors representing north (N), northeast (NE), east (E), southeast (SE), south (S),
 932 southwest (SW), west (W), and northwest (NW). The mean (cross), median (horizontal
 933 line), 25th and 75th percentiles (lower and upper box), and 10th and 90th percentiles
 934 (lower and upper whiskers) are shown.



935

936 Fig. 12. PSCF of NR-PM₁ species during four seasons: (a) organics; (b) sulfate;
 937 (c) nitrate; (d) chloride. The cities marked in each panel are Beijing (BJ), Tianjing (TJ),
 938 Langfang (LF), Baoding (BD), Shijiazhuang (SJZ), and Hengshui (HS). The color scales
 939 indicate the values of PSCF.